



Investigation on the pyrolysis and oxidation of toluene over a wide range conditions. II. A comprehensive kinetic modeling study



Wenhai Yuan ^{a,b}, Yuyang Li ^{a,*}, Philippe Dagaut ^{b,*}, Jiuzhong Yang ^c, Fei Qi ^{a,c}

^aState Key Laboratory of Fire Science, University of Science and Technology of China, Hefei, Anhui 230026, PR China

^bC.N.R.S.-I.N.S.I.S., Institut de Combustion, Aérothermique, Réactivité et Environnement, 1C, Avenue de la Recherche Scientifique, 45071 Orléans Cedex 2, France

^cNational Synchrotron Radiation Laboratory, University of Science and Technology of China, Hefei, Anhui 230029, PR China

ARTICLE INFO

Article history:

Received 7 April 2014

Received in revised form 6 July 2014

Accepted 12 July 2014

Available online 5 August 2014

Keywords:

Toluene

Kinetic model

Pyrolysis

Oxidation

ABSTRACT

The flow reactor pyrolysis of toluene from low to atmospheric pressures and jet stirred reactor oxidation of toluene at high pressure have been studied in Part I of this serial work. The targets in this part are to collect and review the experimental data of toluene pyrolysis and oxidation reported in recent years, and validate the kinetic model of toluene combustion developed in Part I. The vast amount of data used in this work mainly include species profiles in shock tube pyrolysis and oxidation, flow reactor oxidation and low pressure premixed laminar flames, and global combustion parameters such as ignition delay times and laminar flame speeds. Along with the validation of new pyrolysis and oxidation data in Part I, a wide range of conditions from low to high temperatures, subatmospheric to high pressures, very lean to pyrolysis conditions were validated in this work. The satisfactory reproduction of these data demonstrates that the present model can be used in combustion simulation of surrogate fuels containing toluene and as a reliable basis to develop kinetic models of large alkylbenzenes and bicyclic aromatics.

© 2014 The Combustion Institute. Published by Elsevier Inc. All rights reserved.

1. Introduction

As the simplest substituted aromatic hydrocarbon, toluene exists naturally in transportation fuels and is considered as an important component in surrogate fuels of gasoline. It also serves as a prototypical fuel to investigate the combustion of large aromatic components in diesel and jet fuels, and is widely used to investigate the formation and growth of polycyclic aromatic hydrocarbons (PAHs). The combustion chemistry of toluene has been of great interest in the last decades. Many experimental studies on the pyrolysis and oxidation of toluene have been performed. A brief introduction of the previous studies has been described in Part I of this serial work [1]. Concentration profiles of species in pyrolysis [2–13], oxidation [14–23] and flames [24–28] of toluene have been measured. Moreover, global combustion parameters such as ignition delay times [21,29–35] and laminar flame speeds [36–42] have also been measured. These experimental measurements cover a wide range of temperatures, pressures and equivalence ratios (ϕ), providing a large body of useful experimental data for the validation of kinetic models of toluene combustion. Based on these experimental results, several kinetic models of

toluene combustion were also developed (see [23]), which have been briefly introduced in Part I [1]. Most of these toluene models concerned on either the pyrolysis or the oxidation, while few of them focused on both pyrolysis and oxidation. Thus a toluene model with comprehensive validation against the pyrolysis and oxidation data of toluene is desired.

The goal of this work is to collect and review the vast amount of experimental data about the pyrolysis and oxidation of toluene, and further validate a toluene model developed in Part I using the experimental data at a wide range of conditions. Table 1 summarizes the experimental investigations on toluene pyrolysis and oxidation analyzed in this work. The present model can be used for constructing the kinetic models of gasoline surrogate fuels and as a starting point for the development of kinetic models of large alkylated aromatic fuels and bicyclic aromatic fuels. Moreover, the benzyl chemistry and the sub-mechanisms of benzene and 1,3-cyclopentadiene were also validated against previous experimental data of benzyl decomposition, benzene combustion and 1,3-cyclopentadiene combustion with consideration of their important roles in toluene models. Modeling analyses were performed to investigate the chemistry in fuel decomposition process and provide insight into the aromatic growth process which includes the growth of monocyclic aromatic hydrocarbons (MAHs) and the formation and growth of PAHs.

* Corresponding authors.

E-mail addresses: yuygli@ustc.edu.cn (Y. Li), dagaut@cnrs-orleans.fr (P. Dagaut).

Table 1

Summary of the experimental investigations on toluene pyrolysis and oxidation analyzed in this serial work.

Experimental type	Temperature	Pressure	Equivalence ratio	Feed composition	References
Flow reactor	1173 K	1 atm	0.76	1514 ppm in O ₂ /N ₂	[17]
	1100–1730 K	5–760 Torr	∞	5% mol in Ar	[1]
Shock tube (Species profiles)	1150–2200 K	0.2–0.5 atm	∞	1.8% mol in Ne	[3]
	1300–1800 K	1.5–7.8 bar	∞	2–30 ppm in Ar	[74]
	1350–1900 K	0.1–2 bar	∞	0.1–5.67 ppm in Ar	[5]
	1200–1850 K	10 atm	∞	1% mol in Ar	[4]
	1210–1480 K	22–550 bar	1.0, 5.0	8–85 ppm in O ₂ /Xe/Ar	[20]
	1200–1900 K	27, 45 bar	∞	104 ppm in Ne	[6,7]
Jet stirred reactor	873–923 K	1 bar	0.45–0.91	1.4–1.7% in He	[21]
	1000–1400 K	1 atm	0.5, 1.0, 1.5	0.15% mol in N ₂	[18]
	950–1200 K	10 atm	0.5, 1.0, 1.5	0.10% mol in N ₂	[1]
Laminar premixed flame	500–2200 K	30 Torr	1.90	Toluene/O ₂ /Ar flames	[26]
	500–2200 K	30 Torr	0.75–1.75	Toluene/O ₂ /Ar flames	[27]
	500–1700 K	36 Torr	2.0	Toluene/O ₂ /Ar flames	[25]
	500–1700 K	36 Torr	0.7, 1.0	Toluene/O ₂ /Ar flames	[28]
Laminar flame speeds	T _u = 298 K	1 atm	0.8–1.4	Toluene/air flames	[36]
	T _u = 298 K	1 atm	0.8–1.3	Toluene/air flames	[37]
	T _u = 353 K	1 atm	0.7–1.4	Toluene/air flames	[40]
	T _u = 400 K	1 atm	0.7–1.4	Toluene/air flames	[38]
	T _u = 400 K	1 atm	0.7–1.4	Toluene/air flames	[39]
	T _u = 470 K	1 atm	0.7–1.3	Toluene/air flames	[38]
	T _u = 470 K	1 atm	0.7–1.3	Toluene/air flames	[39]
	T _u = 298–358 K	1 atm	0.7–1.3	Toluene/air flames	[42]
	T _u = 450 K	3 atm	0.8–1.4	Toluene/air flames	[41]
Shock tube (Ignition delay times)	1330–1820 K	2.27–6.81 atm	0.33–1.0	0.5–1.5% mol in O ₂ /Ar	[29]
	1430–1950 K	1.1 atm	0.5–1.5	0.4% mol in O ₂ /Ar	[30]
	1430–1820 K	1 atm	1.0	0.1–1% mol in O ₂ /Ar	[32]
	1110–1420 K	12–50 atm	0.25–1.0	0.58–2.28% mol in O ₂ /N ₂	[34]
	1000–1320 K	50 atm	0.5–1.0	1.15–2.28% mol in O ₂ /N ₂	[31]
Rapid compression machine	920–1100 K	50 atm	0.5–1.0	0.96% mol in O ₂ /N ₂ /Ar	[33]

2. Kinetic model and validation of benzyl chemistry and sub-mechanisms of benzene and 1,3-cyclopentadiene

2.1. Kinetic model

The kinetic model used in this work consists of 272 species and 1698 reactions. The reaction mechanism consists of the sub-mechanisms of toluene (A1CH₃, nomenclature in the present model), benzene (A1), 1,3-cyclopentadiene (C₅H₆), C₀–C₄ species and C₈ and larger aromatic species. The reaction mechanism, thermodynamic data and transport data are provided in the *Supplementary Materials* of Part I [1]. The construction of the toluene sub-mechanism and the sub-mechanism of C₈ and large aromatic species has been introduced in detail in Part I [1]. In this section, the construction of the sub-mechanisms of A1, C₅H₆ and C₀–C₄ species will be introduced. **Table S1 in the Supplementary Materials** lists the molecular weights, formulas, names, nomenclatures in this model and molecular structures for the C₅ and larger species mentioned below. Chemkin-Pro software [43] was used for the numerical simulation, and the detailed modules used in the simulation will be introduced in the following sections.

2.1.1. Benzene sub-mechanism

Benzene can be produced at high concentration levels in toluene combustion [9,26,27]. The rate constant of the unimolecular decomposition reaction of A1 to produce phenyl radical (A1–) + H was taken from the model of Wang and Frenklach [44]. The rate constants of H-atom abstraction reactions of A1 by H and methyl radical (CH₃) were adopted from the model of Emdee et al. [16] and the theoretical work of Tokmakov et al. [45], respectively. The rate constant of unimolecular decomposition reaction of A1– to produce benzene (*o*-C₆H₄, R1) was taken from the model of Wang and Frenklach [44]. For the unimolecular decomposition of

o-C₆H₄ to produce diacetylene (C₄H₂) + acetylene (C₂H₂) (R2), the rate constant was taken from the theoretical work of Moskaleva et al. [46]. The rate constants of reactions between A1 and OH to produce A1– + H₂O and phenol (A1OH) + H were taken from the experimental work of Seta et al. [47] and the model of Sakai et al. [48], respectively. The rate constant of H-atom abstraction of A1 by O was adopted from the model of Alzueta et al. [49], and the rate constants of other reactions between A1 and O were taken from the theoretical study of Taatjes et al. [50]. A1– can react with O₂ to produce phenoxy radical (A1O) + O (R3) and *ortho*-benzoquinone (*o*-C₆H₄O₂) + H (R4). Frank et al. [51] determined the rate constants of (R3) and (R4) using atomic and molecular resonant absorption spectroscopy behind shock waves, and their results were used in this model. Moreover, the rate constant of unimolecular decomposition of A1O to produce cyclopentadienyl radical (C₅H₅) + CO (R5) was taken from the theoretical work of You et al. [52].



2.1.2. 1,3-Cyclopentadiene sub-mechanism and C₀–C₄ sub-mechanism

C₅H₆ and C₅H₅ are also important intermediates in toluene combustion [9,26,27]. The rate constants of unimolecular decomposition of C₅H₅ to propargyl radical (C₃H₃) + C₂H₂ (R6) and its isomerization to a linear C₅H₅ structure were taken from the

theoretical investigation of Moskaleva and Lin [53]. The reactions between C_5H_5 and CH_3 can produce methylcyclopentadiene ($C_5H_5CH_3$), methylcyclopentadienyl radical ($C_5H_4CH_3$) + H (R7) and methylenecyclopentadiene radical ($C_5H_5CH_2$) + H. The further decomposition of $C_5H_4CH_3$ and $C_5H_5CH_2$ can produce fulvene. Sharma and Green [54] have performed a comprehensive theoretical study on the reactions between C_5H_5 and CH_3 , and their calculated rate constants were used in this model. Furthermore, Zhong and Bozzelli [55] and Robinson and Lindstedt [56] have investigated the oxidation reactions of C_5H_5 , and their calculated rate constants were also used in this model.



The C_0 – C_4 sub-mechanism used in this work was taken from our recent combustion models of butanol isomers [57,58] which have been validated against a variety of pyrolysis and oxidation data in different reactors and over a wide range of conditions.

2.2. Validation of benzyl chemistry and sub-mechanisms of benzene and 1,3-cyclopentadiene

2.2.1. Validation of benzyl chemistry

The thermal decomposition experiments of benzyl halides in shock tube have been performed by Oehlschlaeger et al. [59] and Sivaramakrishnan et al. [60]. The concentration–time traces of H and benzyl radical ($A1CH_2$) were measured, which provide valuable validation data for the initial decomposition kinetics of $A1CH_2$. Thus the time traces of $A1CH_2$ in the pyrolysis of benzyl iodide ($A1CH_2I$) [59] and those of H and D atoms in the pyrolysis of benzyl bromide ($A1CH_2Br$) and benzyl bromide, α -d2 ($A1CD_2Br$) [60] were simulated with the present model. The simulation was performed with the Closed Homogeneous Batch Reactor module in the Chemkin-Pro software [43], and the shock tube was treated as a zero-dimensional adiabatic reactor with constant volume.

Same simulation method was used in the following shock tube simulations, and will not be repeated therein.

Figure 1 shows the experimental and simulated time traces of $A1CH_2$, H and D. The corresponding experimental conditions in [59,60] are listed in the figure caption. To simulate the decomposition of $A1CH_2I$ and $A1CH_2Br$, the reactions $A1CH_2I = A1CH_2 + I$ and $A1CH_2Br = A1CH_2 + Br$ from [59,60] were added to this model. To simulate the decomposition of $A1CD_2Br$, a simple mechanism of $A1CD_2Br$ including reactions of $A1CD_2Br$, $A1CD_2$ and deuterated products was added, and the rate constants were taken from the same type reactions of corresponding undeuterated species. It can be observed from **Fig. 1** that this model can reproduce the experimental time traces of $A1CH_2$, H and D reasonably well. The sensitivity analysis was performed at the condition of **Fig. 1(b)** to reveal the most influential reactions for the formation and consumption of H atom, as shown in **Fig. 2**. It can be seen that the decomposition reaction of $A1CH_2$ to produce fulvenallene (C_7H_6) + H (R8) shows the largest positive sensitivity to H atom. Other sensitive reactions for H formation are the unimolecular H elimination of C_7H_6 (R9) and pentatetraene (C_5H_4 , R10). Reactions (R11) and (R12) show negative sensitivities to H atom, since the two non-atom producing pathways are the competitive reactions of (R8).



2.2.2. Validation of benzene sub-mechanism

2.2.2.1. Pyrolysis of benzene. Laskin and Lifshitz [61] investigated the thermal decomposition of A1 behind reflected shock waves in

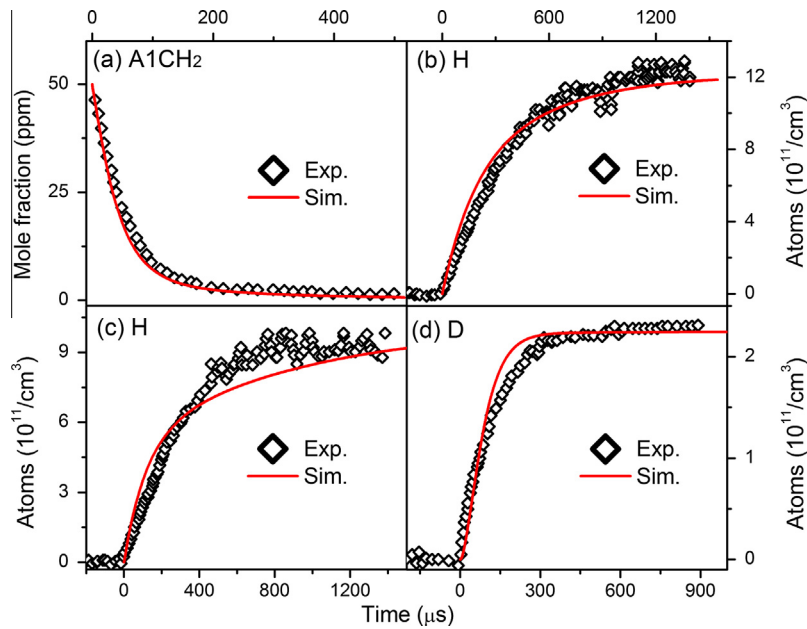


Fig. 1. (a) Experimental (symbols) [59] and simulated (lines) time traces of the benzyl radical in the shock tube pyrolysis of $A1CH_2I$ under conditions: 1615 K, 1.54 bar, 50 ppm $A1CH_2I$ in Ar. (b and d) Experimental (symbols) [60] and simulated (lines) time traces of H and D atoms in the shock tube pyrolysis of $A1CH_2Br$ and $A1CD_2Br$ under conditions: (b) 1573 K, 15.93 Torr, $M_s = 2.515$, $\rho_5 = 3.067 \times 10^{18}$ molecule/cm 3 , $[A1CH_2Br]_0 = 1.585 \times 10^{12}$ molecule/cm 3 ; (c) 1594 K, 15.86 Torr, $M_s = 2.534$, $\rho_5 = 3.074 \times 10^{18}$ molecule/cm 3 , $[A1CD_2Br]_0 = 1.376 \times 10^{12}$ molecule/cm 3 ; (d) 1673 K, 15.94 Torr, $M_s = 2.603$, $\rho_5 = 3.164 \times 10^{18}$ molecule/cm 3 , $[A1CD_2Br]_0 = 1.416 \times 10^{12}$ molecule/cm 3 .

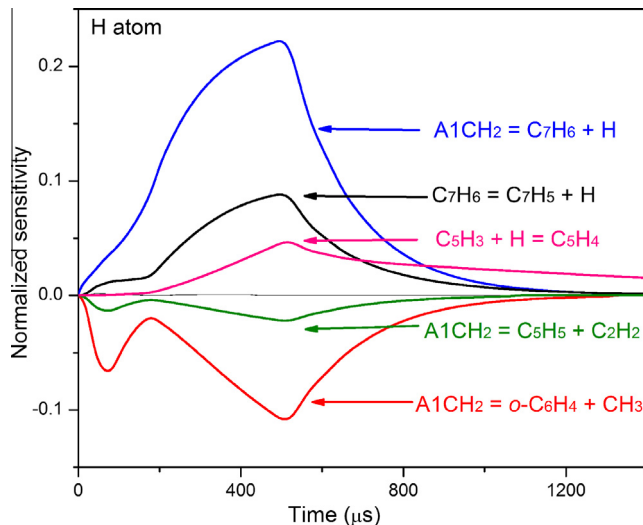


Fig. 2. Sensitivity analysis of H atom in the shock tube pyrolysis of $\text{A1CH}_2\text{Br}$ [60] under the condition: 1573 K, 15.93 Torr, $M_s = 2.515$, $\rho_5 = 3.067 \times 10^{18}$ molecule/cm³.

a single-pulse shock tube at the pressure of ~5 atm, the temperatures of 1400–2000 K and the average reaction time of ~2 ms. **Figure 3** shows the comparison of their experimental results and the simulated results by the present model. Due to the high activation energy to open the benzene ring, the C–H bond dissociation to produce A1^- is the most favorite unimolecular decomposition pathway of A1 at the investigated temperature region. The produced H atoms can drive the H-atom abstraction reaction of A1 which also produces A1^- . At relatively low temperatures, the self-combination reaction to form biphenyl (P2) dominates the consumption of A1^- . As the temperature increases, A1^- tends to be consumed by the β -C–H scission reaction to produce $\text{o-C}_6\text{H}_4$. The ring-opening reaction of $\text{o-C}_6\text{H}_4$ produces great amounts of C_2H_2 and C_4H_2 , making them the major pyrolysis products of A1 at temperatures higher than 1600 K.

2.2.2.2. Oxidation of benzene. Ristori et al. [62] investigated the oxidation of A1 in an atmospheric pressure jet stirred reactor (JSR) at high temperatures, the mean residence time of 0.07 s and a variety of equivalence ratios (0.3, 0.5, 1.0 and 1.5). The simulation

of JSR oxidation was performed with the Perfectly Stirred Reactor module in the Chemkin-Pro software [43]. Same simulation method was used in the following JSR simulations. **Figure 4** compares the experimental data and the simulation results by the present model at 1 atm and the equivalence ratio of 1.0. The H-atom abstraction reactions control the consumption of A1. The produced A1^- can be oxidized by O_2 to form A1O and $\text{o-C}_6\text{H}_4\text{O}_2$. The sensitivity analysis shows that the H-atom abstraction reactions of A1 and the decarbonylation reaction of A1O have the highest sensitivities to A1 consumption. The oxidation of A1 at other equivalence ratios (0.3, 0.5 and 1.5) was also simulated with the present model. The comparisons of experimental and simulated mole fraction profiles are shown in Figs. S1–S3 in the Supplementary Materials.

Marchal et al. [63] investigated the JSR oxidation of A1 at the pressure of 10 atm, the residence time of 0.7 s and a variety of equivalence ratios (0.5, 1.0 and 1.5). The experimental data were also used to validate the benzene sub-mechanism in this model. The experimental and simulated mole fraction profiles of oxidation species are presented in Figs. S4–S6 in the Supplementary Materials.

2.2.2.3. Pyrolysis and oxidation of phenol. A1OH is a significant intermediate in the oxidation of A1. The chemistry of A1OH in the benzene sub-mechanism was also validated against the available experimental work on the pyrolysis and oxidation of A1OH . Lovell et al. [64] and Brezinsky et al. [65] investigated the pyrolysis and oxidation of A1OH in an atmospheric pressure flow reactor at ~1170 K, respectively. According to their experimental results, CO, C_5H_6 and A1 are the major products in the pyrolysis and oxidation of A1OH . In this work, their experimental results were simulated using the Closed Homogeneous Batch Reactor module in the Chemkin-Pro software [43], and the flow reactor was treated as an adiabatic and isobaric homogeneous batch reactor. Same simulation method was used in the following flow reactor simulations. The simulated results were shifted –20 ms for the $\phi = 1.73$ condition to justify the change of reactivity caused by the radical diffusion and mixing effect in the diffuser section. The comparison of experimental mole fraction profiles and simulated results is presented in Fig. S7 in the Supplementary Materials. The present model is able to capture the decomposition of A1OH and the formation of CO and C_5H_6 . However it under-predicts the formation of A1 under the pyrolysis condition and over-predicts the concentrations of A1 under the oxidation conditions.

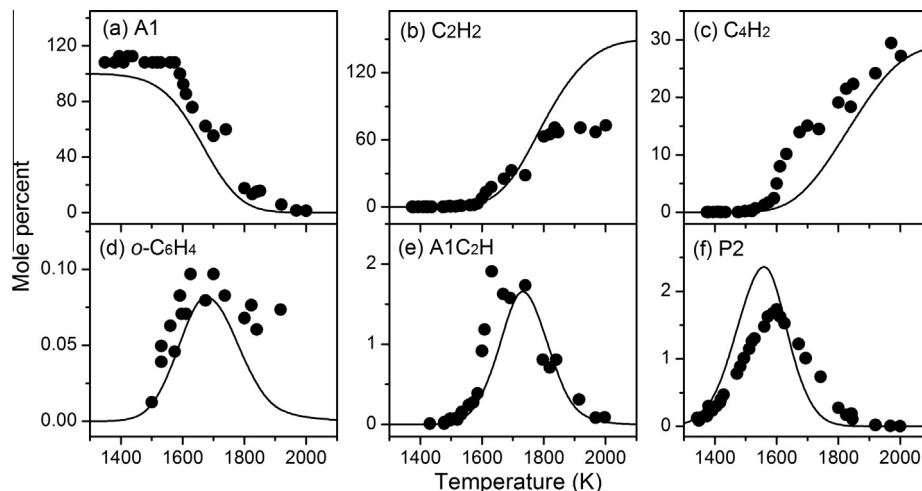


Fig. 3. Experimental (symbols) [61] and simulated (lines) mole fraction profiles of benzene (A1), acetylene (C_2H_2), diacetylene (C_4H_2), benzyne ($\text{o-C}_6\text{H}_4$), phenylacetylene ($\text{A1C}_2\text{H}$) and biphenyl (P2) in the shock tube pyrolysis of benzene at ~5 atm and the average reaction time of 2 ms.

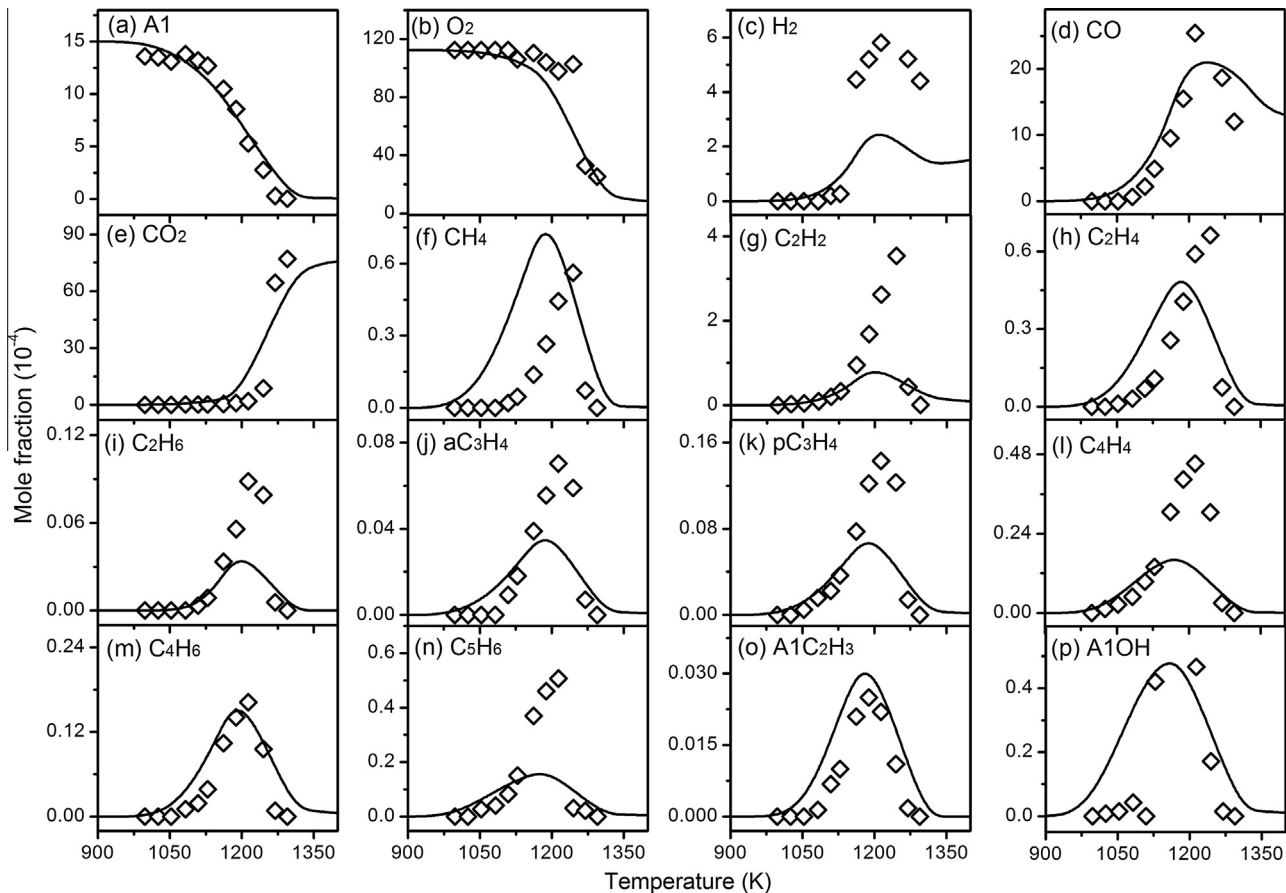
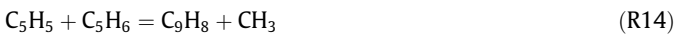


Fig. 4. Experimental (symbols) [62] and simulated (lines) mole fraction profiles of benzene (A1), O₂, H₂, CO, CO₂, methane (CH₄), acetylene (C₂H₂), ethylene (C₂H₄), ethane (C₂H₆), allene (aC₃H₄), propyne (pC₃H₄), vinylacetylene (C₄H₄), 1,3-butadiene (C₄H₆), 1,3-cyclopentadiene (C₅H₆), styrene (A1C₂H₃) and phenol (A1OH) in the JSR oxidation of benzene at $\phi = 1.00$, $P = 1$ atm, $\tau = 0.07$ s.

2.2.3. Validation of 1,3-cyclopentadiene sub-mechanism

2.2.3.1. Pyrolysis of 1,3-cyclopentadiene. Kim et al. [66] studied the flow reactor pyrolysis of C₅H₆ at the pressure of 1 atm, the temperatures of 800–1200 K and the nominal residence time of 3 s. Some aromatic products were observed. Figure S8 shows the experimental and simulated mole fraction profiles of C₅H₆ and major aromatic products. The agreement between experimental and simulated results of C₅H₆ is good. The present model can also reproduce the formation of indene (C₉H₈), naphthalene (A2) and phenanthrene (A3), while it under-predicts the formation of styrene (A1C₂H₃) and A1 by about a factor of 2. The ROP analysis performed at 1100 K shows that over half of C₅H₆ is consumed by H-atom abstraction to produce C₅H₅. Other important consumption pathways of C₅H₆ are the reactions with C₅H₅ to produce A2 (R13), C₉H₈ (R14), A1 (R15) and A1C₂H₃ (R16). The high yields of aromatic products in the pyrolysis of C₅H₆ and the high contributions of (R13), (R14), (R15), (R16) to the consumption of C₅H₆ confirm the significant role of combination reactions between C₅ species in the C₅H₆ sub-mechanism.



Butler and Glassman [67] investigated the flow reactor pyrolysis of C₅H₆ at atmospheric pressure. Two pyrolytic conditions were validated using the present model: 3000 ppm by volume (ppmv)

C₅H₆ at 1150 K and 2077 ppmv C₅H₆ at 1202 K. Figure 5 illustrates the comparison of experimental and simulated mole fraction profiles of C₅H₆, C₁–C₄ pyrolysis products and some aromatic products as the function of residence time. The simulated results were shifted –5 and –25 ms for the 1150 and 1202 K conditions respectively to justify the change of reactivity caused by the radical diffusion and mixing effect in the diffuser section. The ROP analysis was performed for the 1202 K condition. Nearly 70% of C₅H₆ is consumed via the H-atom abstraction reactions by H and CH₃. The rest of C₅H₆ mainly reacts with C₅H₅ to produce some aromatic species, especially A2. Most of C₅H₅ is also consumed to produce A2. Thus A2 is the most abundant product in the pyrolysis of C₅H₆, as illustrated in Fig. 5(l). Besides the aromatic products observed by Kim et al. [66], toluene was detected with very low concentrations in the pyrolysis of C₅H₆ by Butler and Glassman [67], as presented in Fig. 5(i).

Most recently, Djokic et al. [68] investigated the flow reactor pyrolysis of C₅H₆ under both low (16.7% C₅H₆ in N₂) and high (4% C₅H₆ in N₂) dilutions. The experiments were performed at the pressure of 1.7 bar and the temperatures of 873–1123 K. Major pyrolysis products were detected, including some PAHs. The experimental results were also simulated by the present model using the Plug Flow Reactor module in the Chemkin-Pro software [43]. The comparisons of experimental and simulated concentration profiles of C₅H₆ and its pyrolysis products are presented in Figs. S9 and S10 in the Supplementary Materials.

2.2.3.2. Oxidation of 1,3-cyclopentadiene. The oxidation experiments of C₅H₆ performed by Butler and Glassman [67] were also simulated using the present model. Two conditions were simulated: one is 3097 ppmv C₅H₆, 1151 K and equivalence ratio of 1.01; the

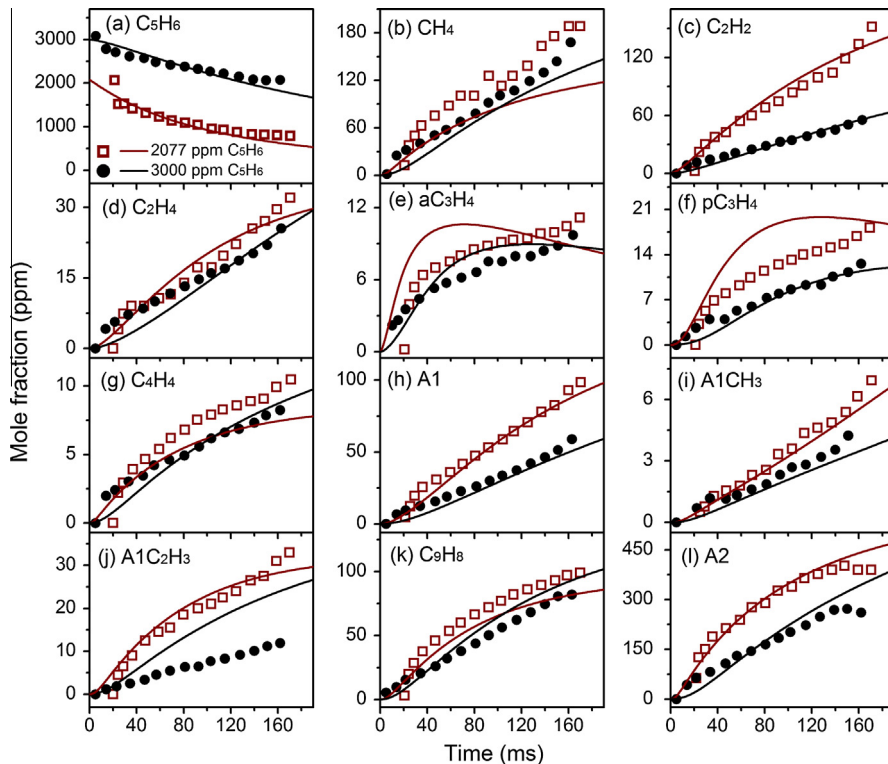


Fig. 5. Experimental (symbols) [67] and simulated (lines) mole fraction profiles of cyclopentadiene (C_5H_6), methane (CH_4), acetylene (C_2H_2), ethylene (C_2H_4), allene (aC_3H_4), propyne (pC_3H_4), vinylacetylene (C_4H_4), benzene (A1), toluene (A1CH₃), styrene (A1C₂H₃), indene (C_9H_8) and naphthalene (A2) in the atmospheric pressure flow reactor pyrolysis of cyclopentadiene. Solid symbols: 3000 ppmv C_5H_6 , $T = 1150$ K; hollow symbols: 2077 ppmv C_5H_6 , $T = 1202$ K.

other one is 2242 ppmv C_5H_6 , 1198 K and $\phi = 1.03$. The experimental and simulated mole fraction profiles of C_5H_6 , C_1 - C_4 oxidation products and some aromatic products are shown in Fig. S11. Similar to the pyrolysis simulation in last section, the simulated results were shifted –5 and –15 ms for the 1151 and 1198 K conditions respectively to justify the change of reactivity caused by the radical diffusion and mixing effect in the diffuser section.

The ROP analysis was performed for the 1198 K condition. C_5H_6 is mainly consumed by the H-atom abstraction reactions to produce C_5H_5 . Besides, the oxidation reactions of C_5H_6 by OH and O to produce 1,3-butadiene (C_4H_6) are also important consumption pathways of C_5H_6 , which contribute about 12% together. Thus it can be seen from Fig. S11(g) that C_4H_6 has relatively high concentrations. The dominant consumption pathway of C_5H_5 is the reaction with O_2 to produce 2,4-cyclopentadiene-1-one (C_5H_4O , R17). The subsequent decomposition of C_5H_4O produces vinylacetylene (C_4H_4 , R18) and but-2-yn-1-yl radical (nC_4H_5 , R19). The oxidation of C_4H_4 mainly produces allyl radical (aC_3H_5 , R20), and the subsequent decomposition of aC_3H_5 is the major source for the formation of allene (aC_3H_4) and propyne (pC_3H_4).



The experimental and simulated results of several aromatic products are shown in Fig. S11(h–l). The main formation pathways of A1 are also different from those under the pyrolysis conditions. The ROP analysis shows that most of A1 comes from the reaction sequence $C_5H_5 \rightarrow C_5H_5CH_3 \rightarrow C_5H_4CH_3 \rightarrow$ fulvene \rightarrow A1, since CH_3 is greatly formed through oxidation reactions which can be

revealed by the high concentrations of methane (CH_4). Under the oxidation conditions, A1C₂H₃ is mainly formed by the reaction between C_5H_5 and C_3H_3 , which is different from the situation in pyrolysis. Further analysis shows that under the oxidation conditions, C_3H_3 can be abundantly produced by the reaction sequence from C_5H_5 via (R17), (R18), (R20) etc. ($C_5H_5 \rightarrow C_5H_4O \rightarrow C_4H_4 \rightarrow aC_3H_5 \rightarrow aC_3H_4/pC_3H_4 \rightarrow C_3H_3$). This can explain the increasing importance of $C_5H_5 + C_3H_3$ reaction in the formation of A1C₂H₃ compared with the situations in the pyrolysis. The main formation pathways of C_9H_8 and A2 are very similar to those under the pyrolysis conditions, thus will not be discussed herein.

2.2.3.3. Ignition delay times and laminar flame speeds of 1,3-cyclopentadiene. Orme et al. [69] investigated the ignition delay times of C_5H_6 in shock tube at the pressure of 1 atm, the temperatures of 1300–2200 K and the equivalence ratios of 0.5, 1.0 and 2.0. Their measured ignition delay times were also simulated by the present model. The comparison of experimental and simulated results is shown in Fig. 6(a). The present model can well predict the ignition delay times of C_5H_6 at $\phi = 0.5$ and 1.0, and slightly under-predicts the ignition delay times at $\phi = 2.0$. Ji et al. [70] determined the laminar flame speeds of C_5H_6 in a counterflow configuration at 1 atm with the initial temperature of 353 K. Figure 6(b) presents the comparison of the experimental and simulated results. Generally the model can reproduce the experimental results within the experimental uncertainties, except the slight over-prediction at the rich side.

3. Model validation against experimental data of toluene pyrolysis and oxidation in literature

The validation of this model against previous experimental data of toluene pyrolysis and oxidation is presented in the following order:

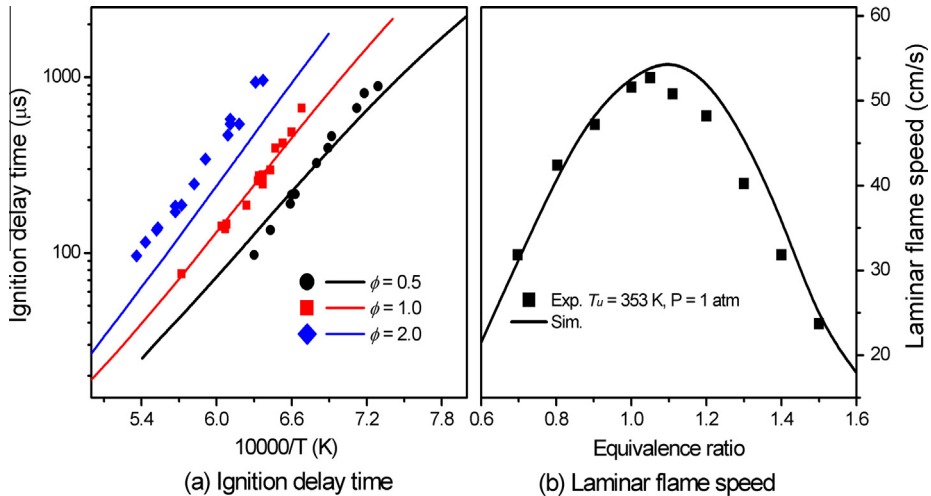


Fig. 6. (a) Experimental (symbols) [69] and simulated (lines) ignition delay times of cyclopentadiene at 1 atm and equivalence ratios of 0.5, 1.0 and 2.0; (b) Experimental (symbols) [70] and simulated (line) laminar flame speeds of cyclopentadiene at 1 atm and the initial temperature of 353 K.

- (1) High pressure pyrolysis in shock tube;
- (2) Oxidation in shock tube;
- (3) Oxidation in jet stirred reactor at low temperature;
- (4) Oxidation in atmospheric pressure flow reactor;
- (5) Oxidation in low pressure premixed flames;
- (6) Ignition delay times in shock tube and rapid compression machine;
- (7) Laminar flame speeds.

3.1. High pressure pyrolysis in shock tube

Colket and Seery [4] investigated the shock tube pyrolysis of 1% toluene in Ar at the pressure of ~ 10 atm, the temperatures of 1200–1850 K and the reaction time of 600 μs . Mole fraction profiles of many stable species from H_2 to pyrene (A4) were measured, and are shown in Fig. 7 along with the simulated results using this model. It can be seen that this model can reproduce the decomposition of A1CH_3 and the formation of major products within the experimental uncertainties. The ROP analysis and the sensitivity analysis were performed at 1500 K, corresponding to about 50% toluene conversion. The results show that about 60% of A1CH_3 is consumed by the H-atom abstraction reaction (R21) to produce $\text{A1CH}_2 + \text{H}_2$, 13% by the unimolecular decomposition reaction (R22) to produce $\text{A1CH}_2 + \text{H}$ and 9% by the ipso-substitution reaction (R23) to produce $\text{A1} + \text{CH}_3$. The sensitivity analysis in Fig. 8 demonstrates that (R21) is the most sensitive reaction for the consumption of A1CH_3 .



The subsequent decomposition of A1CH_2 is mainly via the unimolecular decomposition reactions to produce $\text{C}_7\text{H}_6 + \text{H}$ and $\text{o-C}_6\text{H}_4 + \text{CH}_3$. Figure 8 also shows that the unimolecular decomposition reactions of A1CH_2 have large negative sensitivities to A1CH_3 , since A1CH_2 is the most important decomposition product of A1CH_3 . The subsequent decomposition of C_7H_6 mainly forms fulvenallenyl radical (C_7H_5) via unimolecular C–H fission or H-atom abstraction reactions. About 50% of C_7H_5 decomposes to $\text{C}_4\text{H}_2 + \text{C}_3\text{H}_3$, and 20% is self-combined to form A3, which is similar to the situation in the flow reactor pyrolysis in Part I [1]. C_7H_6 can also suffer a minor decomposition pathway, that is,

unimolecular C–C fission to form cyclopentadienylidene (cC_5H_4) + C_2H_2 . Two main consumption pathways of $\text{o-C}_6\text{H}_4$ are the unimolecular decomposition reaction to produce $\text{C}_4\text{H}_2 + \text{C}_2\text{H}_2$ and the cycloaddition reaction with A1 to form a bicyclic intermediate benzobicyclo[2.2.2]octatriene (BICYCLO, R24) which can decompose to A2 and C_2H_2 (R25). The later pathway was proposed by Comandini et al. [71,72].



A1 is abundantly produced in the pyrolysis of A1CH_3 , as illustrated in Fig. 7. The ipso-substitution of A1CH_3 by H (R23) is the dominant formation pathway of A1. Other formation pathways of A1 include the H-atom abstraction reaction of A1CH_3 by A1 – and the self-combination reaction of C_3H_3 (R26). A great deal of A1 participates in the reaction (R24) to form BICYCLO, and the subsequent decomposition of BICYCLO (R25) leads to the production of A2. The main formation pathways of A2 in the shock tube pyrolysis at 10 atm are different from those in the flow reactor pyrolysis in Part I [1]. The ROP analysis shows that in the high pressure shock tube pyrolysis, most of A2 comes from the reaction sequence $\text{o-C}_6\text{H}_4 + \text{A1} \rightarrow \text{BICYCLO} \rightarrow \text{A2} + \text{C}_2\text{H}_2$.



Sivaramakrishnan et al. [6,7] have also investigated the high pressure shock tube pyrolysis of toluene from 1200 to 1900 K. The experiments were performed at 27 and 45 bar with the average reaction time of 2 ms. However, Narayanaswamy et al. [73] found that the simulated temperature needs to be shifted in order to capture the experimental data of Sivaramakrishnan et al. [6,7] during the validation of their toluene model. The reason for the temperature shift is still unknown. In this work, similar temperature shifts (-70 K at 27 bar and -50 K at 45 bar) were also needed. Figures 9 and 10 present the experimental and simulated results of toluene pyrolysis at 27 and 45 bar, respectively.

The ROP analysis was performed at 45 bar and 1500 K, corresponding to about 50% toluene conversion. The main decomposition pathways of A1CH_3 and A1CH_2 are very similar to those in the shock tube pyrolysis at 10 atm, thus are not repeated herein. From Figs. 9 and 10, it can be seen that both the experimental and simulated results show that C_2H_2 , C_4H_2 , CH_4 and A1 are the most abundant pyrolysis products of toluene at the two high pressures. The ROP analysis shows that the formation pathways of CH_4

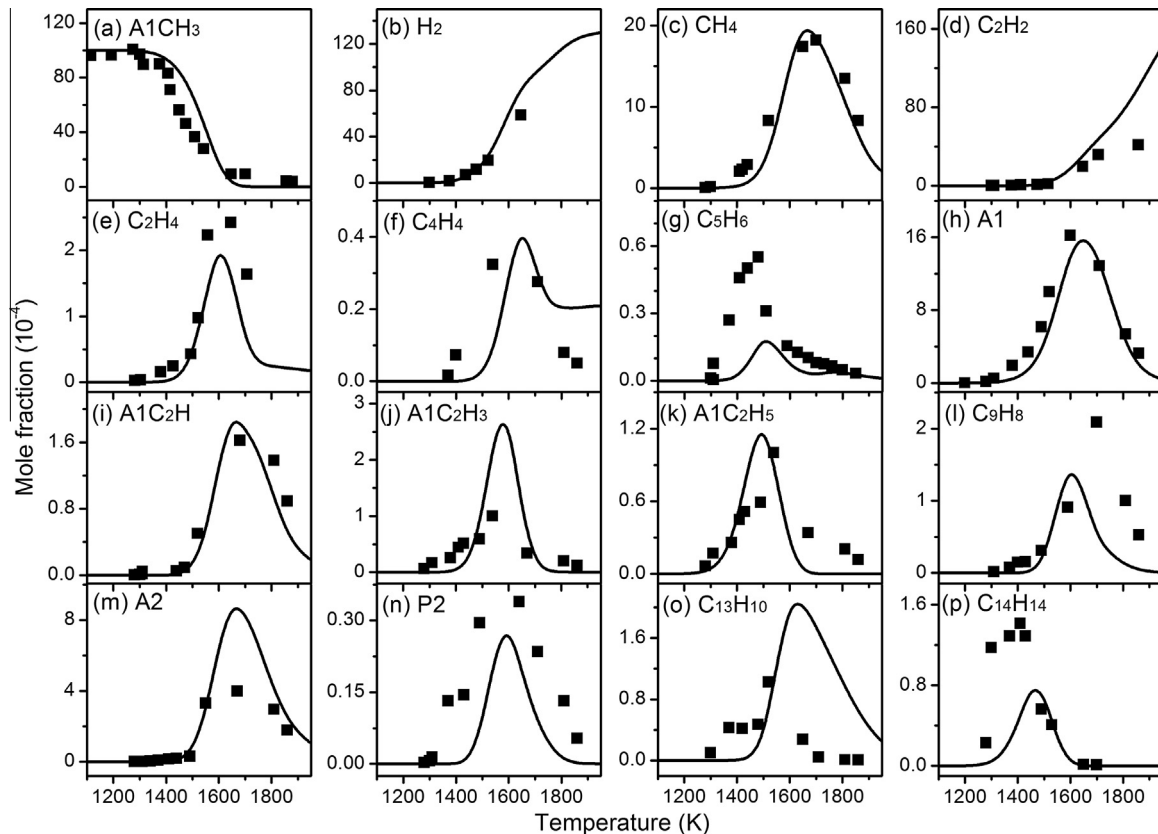


Fig. 7. Experimental (symbols) [4] and simulated (lines) mole fraction profiles of toluene (A1CH₃), hydrogen (H₂), methane (CH₄), acetylene (C₂H₂), ethylene (C₂H₄), vinylacetylene (C₄H₄), 1,3-cyclopentadiene (C₅H₆), benzene (A1), phenylacetylene (A1C₂H), styrene (A1C₂H₃), ethylbenzene (A1C₂H₅), indene (C₉H₈), naphthalene (A2), biphenyl (P2), fluorene (C₁₃H₁₀) and bibenzyl (C₁₄H₁₄) in the shock tube pyrolysis of toluene at total pressures of ~10 atm and residence time near 600 μ s.

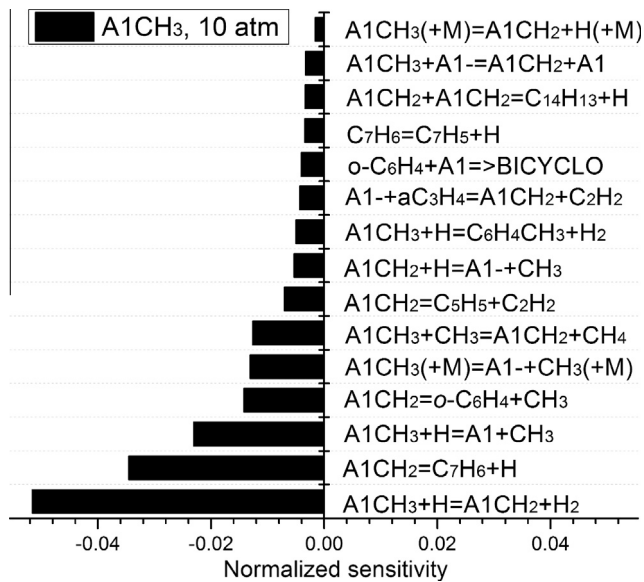


Fig. 8. Sensitivity analysis of toluene (A1CH₃) in the shock tube pyrolysis of toluene at ~10 atm and 1600 K.

and A1 are slightly different from those in the flow reactor pyrolysis in Part I [1]. In this case, over 30% of CH₄ is produced via the H-atom abstraction reaction of C₇H₆ by CH₃, and other pathways are the H-atom abstraction reactions of A1CH₃ and C₅H₆ by CH₃. In the flow reactor pyrolysis case, the dominant formation pathway of CH₄ is the H-atom abstraction reaction of A1CH₃ by CH₃. For A1,

its dominant formation pathway in the flow reactor pyrolysis case is the ipso-substitution of A1CH₃ by H (R23). In this case, (R23) is still dominant, but the role of the self-combination reaction of C₃H₃ (R26) in the formation of A1 is greatly enhanced.

C₂H₂ and C₄H₂ are two most abundant products in the shock tube pyrolysis at 27 and 45 bar. From Figs. 9 and 10, it can be seen that the maximum mole fractions of C₂H₂ are about 8 times higher than those of C₄H₂. About 50% of C₂H₂ is produced from the direct decomposition of A1CH₂ (R12), while the rest mainly comes from the decomposition of C₅H₅ and C₇H₆. The consumption of C₂H₂ mainly forms C₉H₈ (R27) and phenylacetylene (A1C₂H, R28), while the consumption of C₄H₂ mainly forms indenyl radical (C₉H₇, R29).



Furthermore, Pamidimukkala et al. [3] investigated the shock tube pyrolysis of toluene using the time-of-flight mass spectrometry and laser schlieren densitometry. The experiment was performed at 0.2–0.5 atm and 1550–2200 K. Some stable species were detected and the mole fraction profiles of A1CH₃, CH₄, C₂H₂ and C₄H₂ were measured as the function of reaction time. Their experimental results were also simulated using this model and the results are presented in Fig. S12 in the Supplementary Materials.

The present model was also used to simulate the H atom time traces measured by Braun-Unkhoff et al. [74] and Eng et al. [5] in a wide temperature (1465–1705 K) and pressure (0.1–7 bar) range in shock tube. The comparisons of experimental and simulated

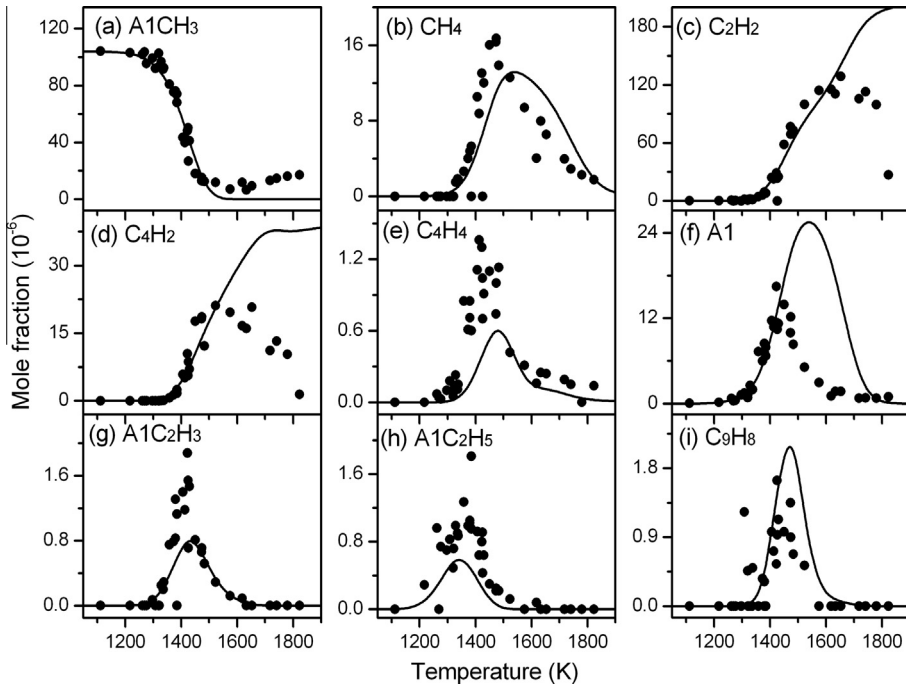


Fig. 9. Experimental (symbols) [6,7] and simulated (lines) mole fraction profiles of toluene (A_1CH_3), methane (CH_4), acetylene (C_2H_2), diacetylene (C_4H_2), vinylacetylene (C_4H_4), benzene (A_1), styrene ($\text{A}_1\text{C}_2\text{H}_3$), ethylbenzene ($\text{A}_1\text{C}_2\text{H}_5$) and indene (C_9H_8) in the shock tube pyrolysis of toluene at 27 bar.

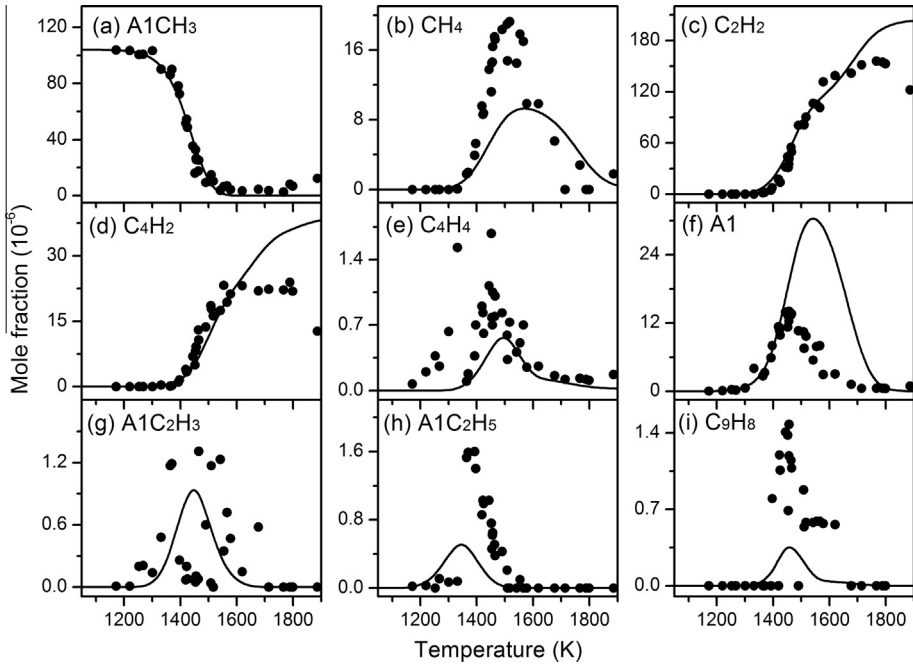


Fig. 10. Experimental (symbols) [6,7] and simulated (lines) mole fraction profiles of toluene (A_1CH_3), methane (CH_4), acetylene (C_2H_2), diacetylene (C_4H_2), vinylacetylene (C_4H_4), benzene (A_1), styrene ($\text{A}_1\text{C}_2\text{H}_3$), ethylbenzene ($\text{A}_1\text{C}_2\text{H}_5$) and indene (C_9H_8) in the shock tube pyrolysis of toluene at 45 bar.

results are provided in Figs. S13 and S14 in the Supplementary Materials.

3.2. Oxidation in shock tube

The time traces of intermediate concentrations are very useful to determine the rate constants of some specific reactions and to validate the initial decomposition and oxidation pathways of fuels. Vasudevan et al. [32] have measured the OH time traces in the

shock tube oxidation of toluene/ O_2/Ar mixtures using narrow-line width ring dye laser absorption spectroscopy. The experiments were performed at 1586–1783 K and 1.79–2.03 atm. Oehlschlaeger et al. [75] have measured the A₁CH₂ time traces in shock-heated toluene/ $\text{O}_2/\text{Ar}/\text{He}$ mixtures using ultraviolet laser absorption of A₁CH₂ at 266 nm. The experiments were performed at the total pressure of ~1.7 bar and a variety of temperatures. In this work, the measured OH and A₁CH₂ time traces in these studies were validated using this model.

Figure 11 presents the experimental and simulated OH time traces at the stoichiometric condition and different temperatures, pressures and argon dilutions. Generally, this model can capture the rises of OH as well as the first plateaus, especially at lower temperatures. The sensitivity analysis shows that the reaction $H + O_2 = O + OH$ has the largest positive sensitivity to the overall production of OH. At early reaction time, OH is mainly produced by the reaction $A1CH_3 + O = A1CH_2 + OH$ and consumed by the reaction $A1CH_3 + OH = A1CH_2 + H_2O$. Meanwhile, the H-atom abstraction of $A1CH_3$ by H (R21) shows negative sensitivity to the formation of OH and the decomposition reaction of $A1CH_2$ shows positive sensitivity.

Figure 12 presents the experimental and simulated $A1CH_2$ time traces at different temperatures, pressures, equivalence ratios and dilutions. It can be seen that this model can get a reasonable prediction of the measured $A1CH_2$ time traces, especially at lower temperatures. At higher temperatures, the simulated $A1CH_2$ time traces are a little slower than the experimental results. From the sensitivity analysis, the reaction between $A1CH_3$ and O_2 (R30) has the largest positive sensitivity, which is in accordance with the findings of Oehlschlaeger et al. [75]. In contrast, the reaction $A1CH_3 + O = cre-sol (HOC_6H_4CH_3)$ shows a negative sensitivity to the formation of $A1CH_2$, since this combination reaction reduces the radical pool and inhibits the formation of $A1CH_2$ via competition.



Sivaramakrishnan et al. [20] studied the high pressure shock tube oxidation of toluene at 22–550 bar and 1210–1480 K. The experiments were performed at stoichiometric and rich ($\phi = 5.0$) conditions with high dilutions. Stable species were detected using gas chromatography (GC) and GC combined with mass spectrometry (GC-MS). **Figure 13** presents the experimental and simulated mole fraction profiles of oxidation species at 22 bar and $\phi = 1.0$ and 5.0. Similar to the simulation of their pyrolysis data in Section 3.1, the simulated results were shifted towards lower temperature region for 50 K. Similar temperature shifts were also used in the simulation work by Metcalfe et al. [23] and Narayanaswamy et al. [73]. It is noticed that the experimental temperature can be well captured by the models of Sivaramakrishnan et al. [22] and Andrae et al. [76,77]. However, as commented by Metcalfe et al. [23], the model of Sivaramakrishnan et al. highly overestimated the rate constant of $A1CH_2 + HO_2$, while the model of Andrae et al. included a lumped radical chain-branching reaction with O_2 , which increases the simulated reactivity of the toluene oxidation system at high pressures. From **Fig. 13**, it can be seen that after the temperature shift, this model can get a reasonable prediction of the decomposition of $A1CH_3$ and the formation of major products.

The ROP analysis at $\phi = 1.0$, 1350 K and $\phi = 5.0$, 1350 K shows that the major pathways in the decomposition and oxidation of $A1CH_3$ are quite similar to those in the jet stirred reactor oxidation at 10 atm in Part I [1]. $A1CH_3$ is consumed mainly by the H-atom abstraction reactions by OH, H and O, producing $A1CH_2$ and methylphenyl radical ($C_6H_4CH_3$). The major difference between $\phi = 1.0$ and $\phi = 5.0$ is that the role of unimolecular decomposition reactions of $A1CH_3$, especially that of (R22), is enhanced at the rich condition. At both equivalence ratios, $A1CH_2$ is mainly consumed by the oxidation reaction by O (R31), unimolecular decomposition reactions (R8), (R12) and unimolecular isomerization reaction (R32). But the dominant consumption pathway is different. At $\phi = 1.0$, (R31) is the most important consumption pathway of $A1CH_2$, while at $\phi = 5.0$ the isomerization reaction (R32) becomes dominant. $C_6H_4CH_3$ is mainly consumed by the reactions with O_2 to produce $o-C_6H_4O_2 + CH_3$ and methylphenoxy radical ($OC_6H_4CH_3 + O$). The former reaction is more preferred at both equivalence ratios. The decomposition of $o-C_6H_4O_2$ mainly decomposes to C_5H_4O . However the dominant decomposition pathway of C_5H_4O in the JSR oxidation is very different from that in the shock tube oxidation. In the shock tube oxidation, over 90% of C_5H_4O decomposes to C_2H_2 and CO through reaction (R33), rather than $C_4H_4 + CO$. The decomposition of $OC_6H_4CH_3$ via the reaction sequence $OC_6H_4CH_3 \rightarrow C_5H_4CH_3 \rightarrow fulvene \rightarrow A1$ ultimately leads to the production of fulvene and A1.



The high pressure shock tube oxidation data of toluene at 50 bar and 550 bar were also simulated. The comparisons of experimental and simulated results are illustrated in **Figs. S15 and S16 in the Supplementary Materials**, respectively.

3.3. Oxidation in jet stirred reactor at low temperature

Bounaceur et al. [21] investigated the JSR oxidation of toluene at 1 atm and lean conditions. The experiments were performed at 873, 893 and 923 K with $\phi = 0.45$ and 0.90. The mole fractions of $A1CH_3$, O_2 and some oxidation products were evaluated as functions of residence time (up to 14 s). In this work, their experimental data at 893 K with $\phi = 0.9$ was simulated using the present model. The experimental and simulated results are shown in **Fig. 14**. The agreements between experimental and simulated results are satisfactory for most of major species, and the reactivity

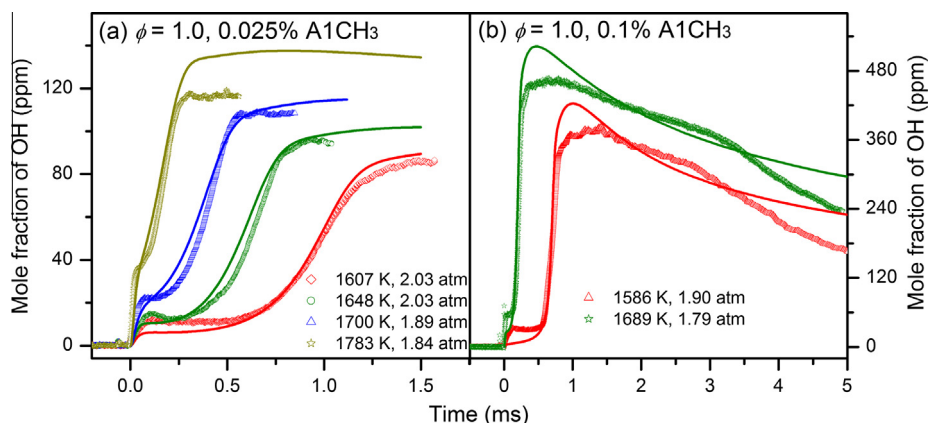


Fig. 11. Experimental (symbols) [32] and simulated (lines) OH concentration profiles at different temperatures, pressures and argon dilutions.

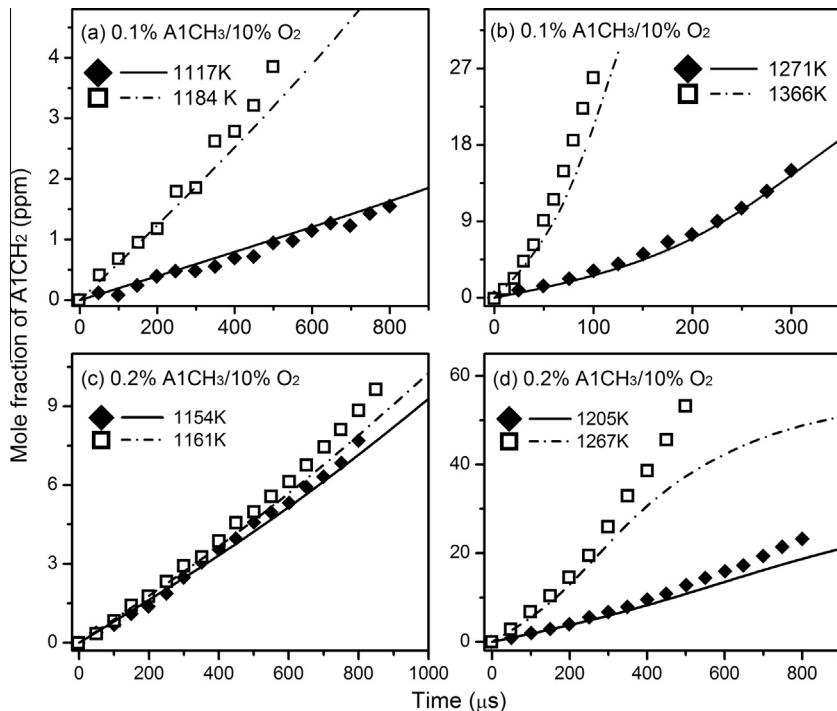


Fig. 12. Experimental (symbols) [75] and simulated (lines) benzyl concentration profiles at different temperatures, equivalence ratios and dilutions.

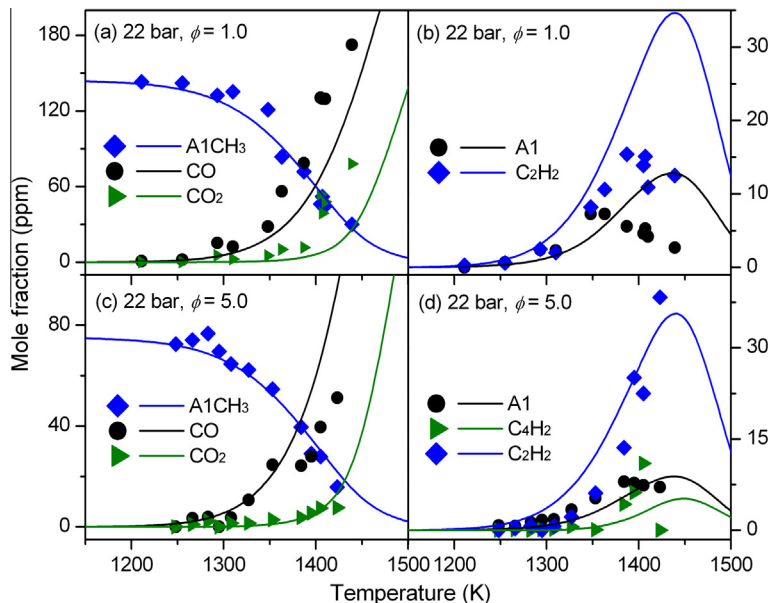


Fig. 13. Experimental (symbols) [20] and simulated mole fraction profiles of toluene (A1CH₃), carbon monoxide (CO), carbon dioxide (CO₂), acetylene (C₂H₂), diacetylene (C₄H₂) and benzene (A1) in the shock tube oxidation of toluene at 22 bar with equivalence ratios of $\phi = 1.0$ and 5.0.

of toluene at the relatively low temperature region can also be captured. The ROP analysis was performed at 893 K, $\phi = 0.9$ and the residence time of 6 s to help understand the low temperature behaviors of toluene. The results show that the main consumption pathways of A1CH₃ are very different from those at higher temperatures in the JSR oxidation studies in Part I [1]. Nearly all of A1CH₃ was consumed by the H-atom abstraction reaction by O₂ (R30) to produce A1CH₂ and HO₂, and the rest is consumed by the H-atom abstraction reaction by HO₂. This big difference can attribute to the longer residence times and lower temperatures which inhibit the

contributions of H-atom abstraction reactions of A1CH₃ by H, O and OH.

A1CH₂ is mainly consumed by the reaction with HO₂ (R34) to produce benzoyl radical (A1CH₂O), and it can also react with A1CH₃ to produce bibenzyl (C₁₄H₁₄, R35). The decomposition of A1CH₂O tends to produce benzaldehyde (A1CHO, R36). It should be noted that the importance of C₆H₄CH₃ and its oxidation reactions decreases in the low temperature JSR oxidation, and they almost have no contributions to the oxidation of toluene. This can be explained by the fact that the dissociation energy of chain

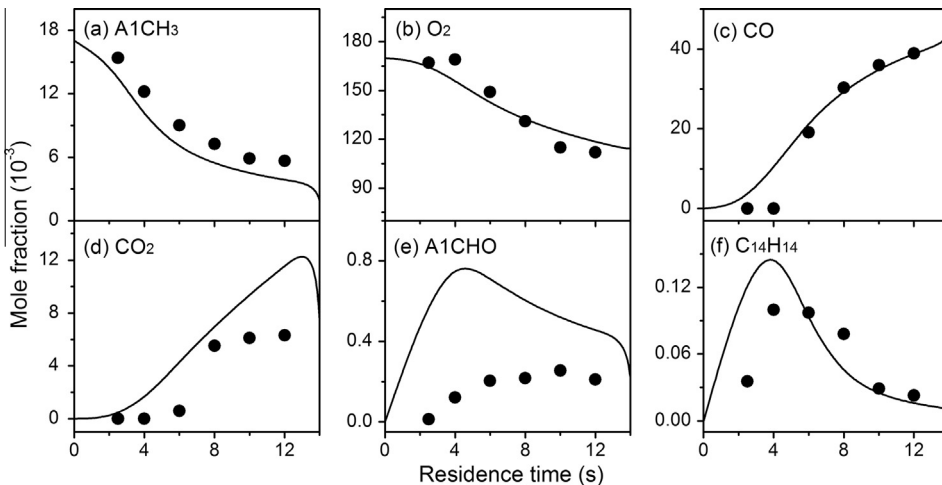


Fig. 14. Experimental (symbols) [21] and simulated (lines) mole fraction profiles of toluene (A1CH₃), oxygen (O₂), carbon monoxide (CO), carbon dioxide (CO₂), benzaldehyde (A1CHO) and bibenzyl (C₁₄H₁₄) in the JSR oxidation of toluene at 893 K and $\phi = 0.9$.

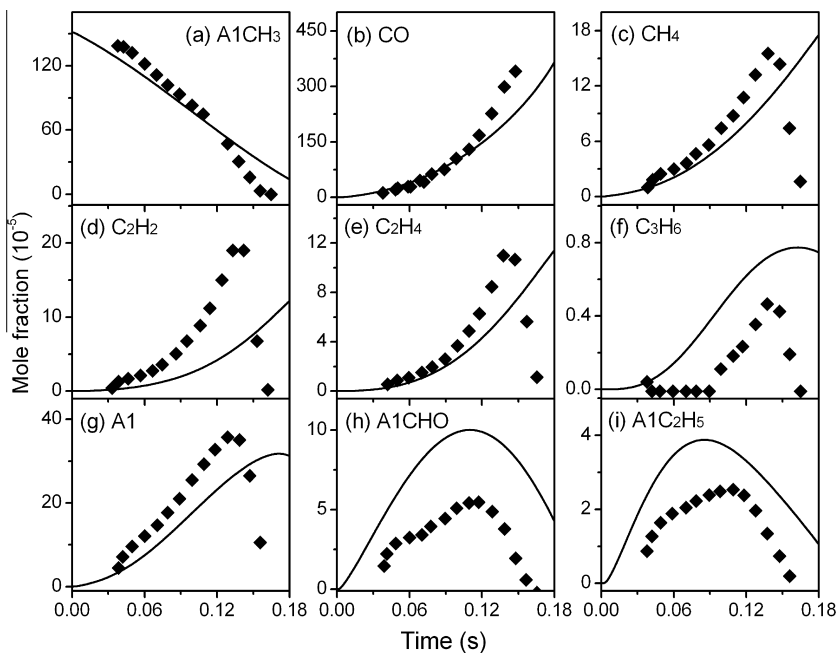


Fig. 15. Experimental (symbols) [17] and simulated mole fraction profiles of toluene (A1CH₃), carbon monoxide (CO), methane (CH₄), acetylene (C₂H₂), ethylene (C₂H₄), propene (C₃H₆), benzene (A1), benzaldehyde (A1CHO) and ethylbenzene (A1C₂H₅) in the atmospheric pressure flow reactor oxidation of toluene at $\phi = 0.73$ and near 1200 K.

C–H bond is much weaker than that of the C–H bonds on the benzene ring [78] and consequently it is much harder to break the C–H bond on the benzene ring at low temperature.



The experimental data at 893 K with $\phi = 0.45$ and at 923 K with $\phi = 0.9$ were also simulated using this model. The experimental and simulated results are shown in Figs. S17 and S18 in the Supplementary Materials. The agreements between experimental and simulated results are satisfactory for most of major species, and the reactivity of toluene can also be captured.

3.4. Oxidation in atmospheric pressure flow reactor

Emdee et al. [16] and Klotz et al. [17] investigated the oxidation of toluene in an atmospheric pressure flow reactor at temperatures around 1200 K with the equivalence ratios from lean to rich

Table 2
Experimental conditions of premixed toluene flames simulated in this work.

ϕ	P/kPa	X_{A1CH_3}	X_{O_2}	X_{Ar}	v (cm/s)	References
0.75	4.0	3.85	46.15	50.00	35.00	[27]
1.00	4.0	5.00	45.00	50.00	35.00	[27]
1.25	4.0	6.10	43.90	50.00	35.00	[27]
1.50	4.0	7.14	42.86	50.00	35.00	[27]
1.75	4.0	8.14	41.86	50.00	35.00	[27]
1.90	4.0	9.98	47.31	42.71	31.50	[26]
0.70	4.7	2.30	29.00	69.00	40.50	[28]
1.00	4.7	2.30	20.00	77.00	40.50	[28]
2.00	4.7	9.90	44.50	45.60	40.50	[25]

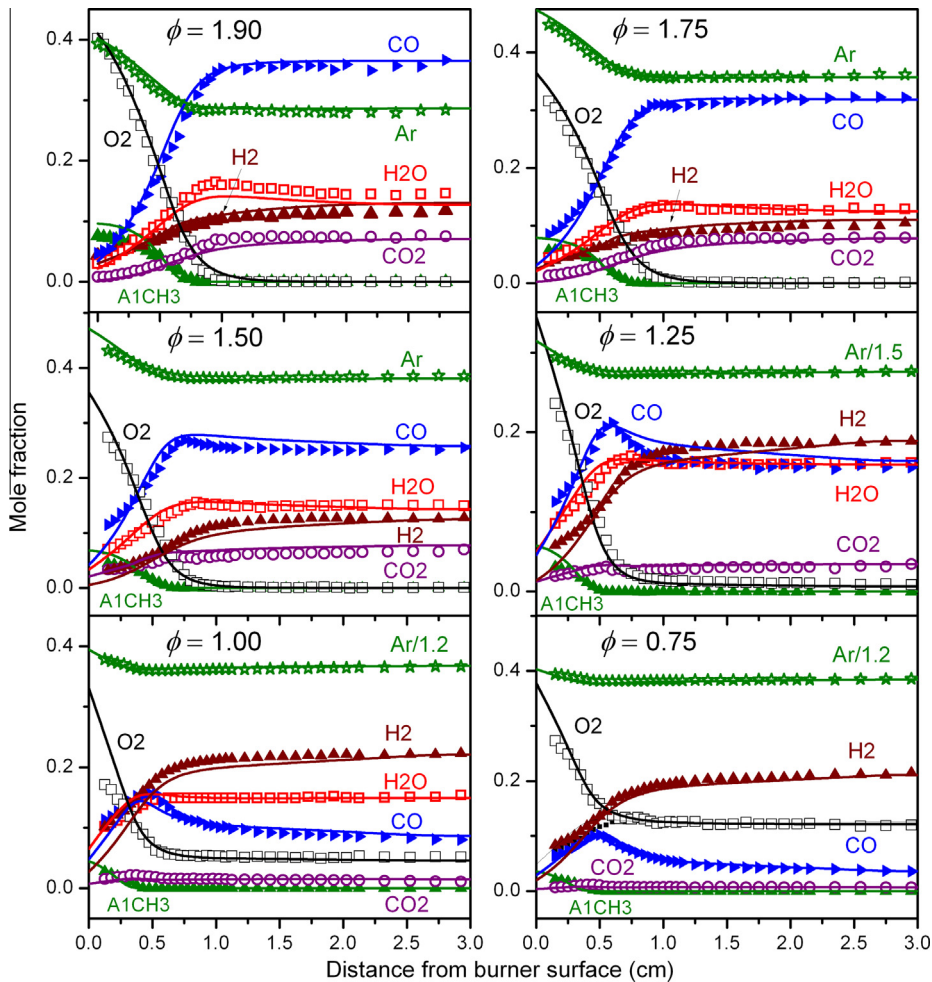


Fig. 16. Experimental (symbols) [26,27] and simulated (lines) mole fraction profiles of major species in the premixed flames of toluene at six equivalence ratios from 0.75 to 1.90.

conditions. The decay of toluene was monitored using GC, and the concentrations of some stable products were measured as the function of residence time. In this work, the oxidation data of toluene [17] ($\phi = 0.76$) was simulated. It should be noted that the experimental residence time had been shifted +30 ms by Klotz et al. [17] to justify the change of reactivity caused by the radical diffusion and mixing effect in the diffuser section. In this work, the experimental data were directly taken from the work of Klotz et al. [17] where the residence time had been shifted +30 ms.

Figure 15 presents the experimental and simulated mole fraction profiles of oxidation species at $\phi = 0.76$ and 1200 K. The ROP analysis shows that the main formation pathways of many major products and intermediates in the flow reactor oxidation are similar to those in the JSR oxidation at close conditions. For example, in the flow reactor oxidation, CO is mainly produced from the unimolecular decomposition of A1O (R37), while A1O mainly comes from the reaction between A1 $-$ and O₂ (R38). A1 is also an abundant product in the flow reactor oxidation of toluene, and has four formation sources with almost equal contributions, i.e. the unimolecular decomposition of C₅H₅CH₂, the isomerization of fulvene, the ipso-substitution of A1CH₃ by H (R23) and the unimolecular decomposition of A1CH₂O (R39). It should be noted that both C₅H₅CH₂ and fulvene come from the reaction sequence C₅H₅ → C₅H₅CH₃ → C₅H₄CH₃/C₅H₅CH₂ → fulvene, which demonstrates once again that the C₅ chemistry plays a crucial role in toluene combustion.



3.5. Oxidation in low pressure premixed flames

There have been two sets of low pressure laminar premixed toluene flames performed in recent years. One was performed by Li et al. [26,27] using synchrotron vacuum ultraviolet photoionization mass spectrometry (SVUV-PIMS), and the other was performed by Detilleux and Vandooren [25,28] using GC and electron-impact ionization mass spectrometry (EIMS). Both sets of flames were performed at near 30 Torr and the equivalence ratios between 0.5 and 2.0. The detailed experimental conditions of these flames are summarized in Table 2. The simulation was performed with the Premixed Laminar Burner-Stabilized Flame module in the Chemkin-Pro software [43], using the reported temperature profiles as input parameters.

Figures 16–19 present the experimental and simulated mole fraction profiles of the major species and important intermediates in the low pressure premixed flames of toluene with the equivalence ratios from 0.75 to 1.90 [26,27]. Figure 20 illustrates the initial reaction pathways of toluene in the $\phi = 1.90$ flame. This model was also validated against the data of Detilleux and Vandooren [25,28] with the equivalence ratios from 0.5 to 2.0, as shown in Figs. S19–S21 in the Supplementary Materials. Generally, the simulated results agree reasonably well with the two sets of experimental

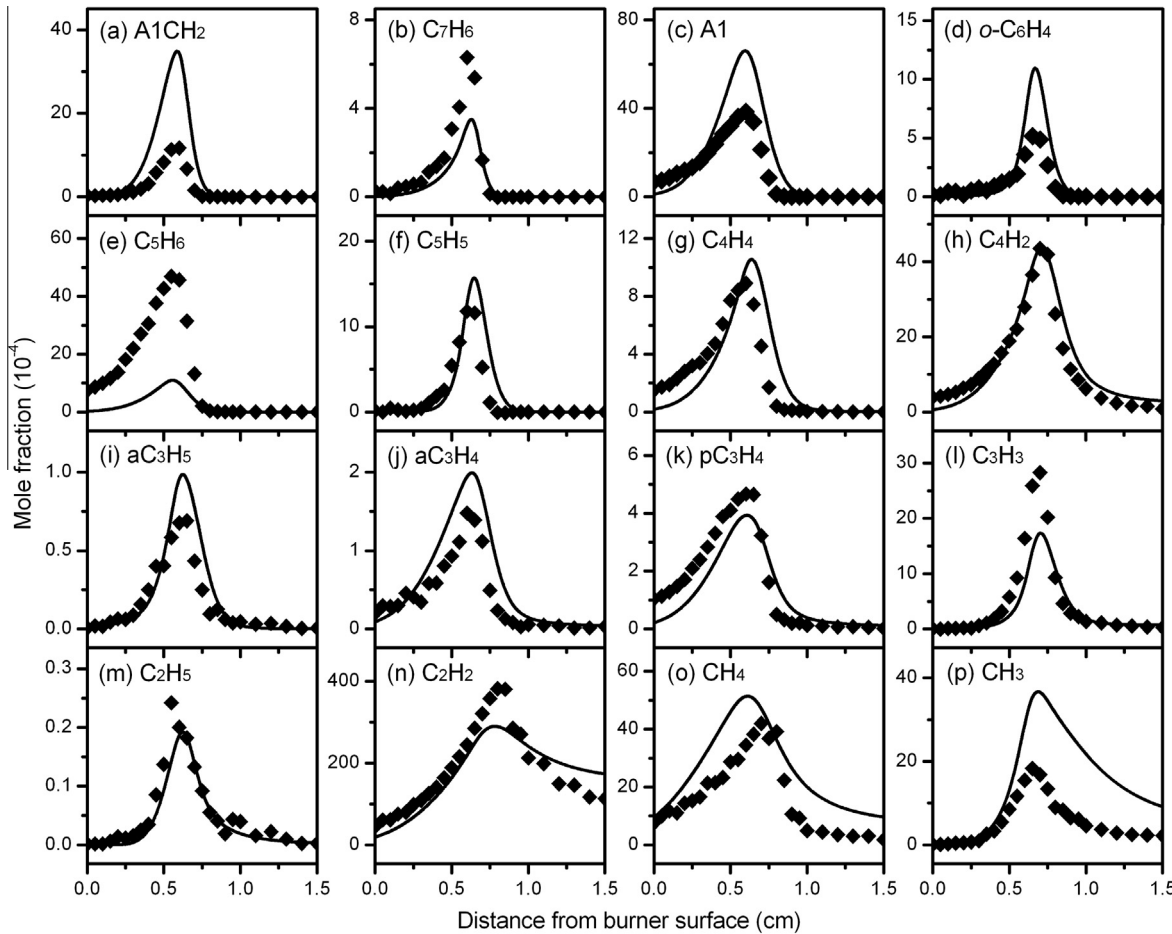


Fig. 17. Experimental (symbols) [26] and simulated (lines) mole fraction profiles of benzyl (A1CH_2), fulvenallene (C_7H_6), benzene (A1), benzyne ($\text{o-C}_6\text{H}_4$), 1,3-cyclopentadiene (C_5H_6), cyclopentadienyl (C_5H_5), vinylacetylene (C_4H_4), diacetylene (C_4H_2), allyl (aC_3H_5), allene (aC_3H_4), propargyl (pC_3H_4), propargyl (C_3H_3), ethyl (C_2H_5), acetylene (C_2H_2), methane (CH_4) and methyl (CH_3) in the premixed flame of toluene at $\phi = 1.90$.

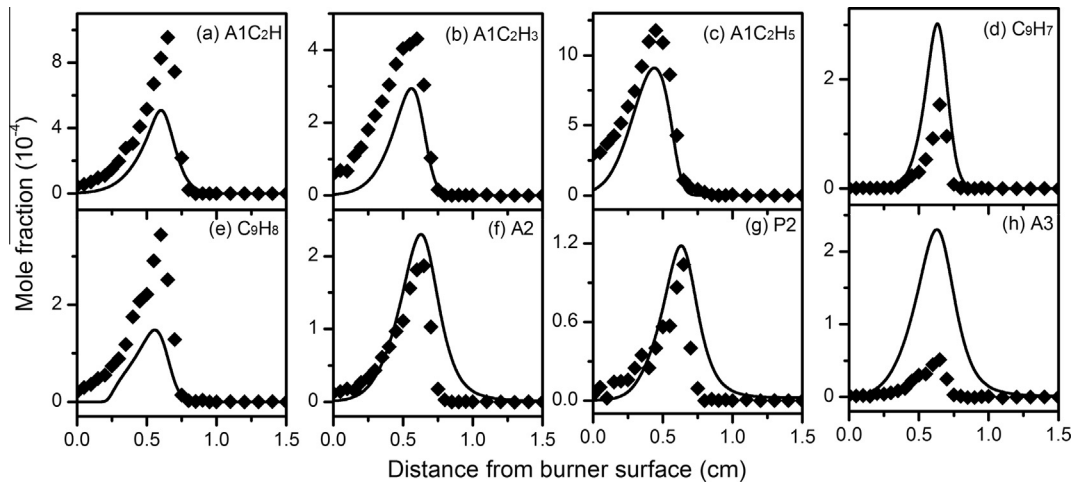


Fig. 18. Experimental (symbols) [26] and simulated (lines) mole fraction profiles of phenylacetylene ($\text{A1C}_2\text{H}$), styrene ($\text{A1C}_2\text{H}_3$), ethylbenzene ($\text{A1C}_2\text{H}_5$), indenyl (C_9H_7), indene (C_9H_8), naphthalene (A2), biphenyl (P2) and phenanthrene (A3) in the premixed flame of toluene at $\phi = 1.90$.

data, which demonstrates the good performance of this model on simulating high temperature oxidation of toluene from lean to rich conditions. A rich ($\phi = 1.90$) flame [26] and a lean ($\phi = 0.75$) flame [27] are selected here to discuss the high temperature oxidation chemistry of toluene in different reaction circumstances.

Figure 17(a-d) shows the experimental and simulated mole fraction profiles of A1CH_2 , C_7H_6 , A1 and $\text{o-C}_6\text{H}_4$ in the $\phi = 1.90$ flame. The most favored decomposition pathways of A1CH_3 in the $\phi = 1.90$ flame are the H-atom abstraction reactions by H , OH and O to produce A1CH_2 . A1CH_2 is further consumed to form

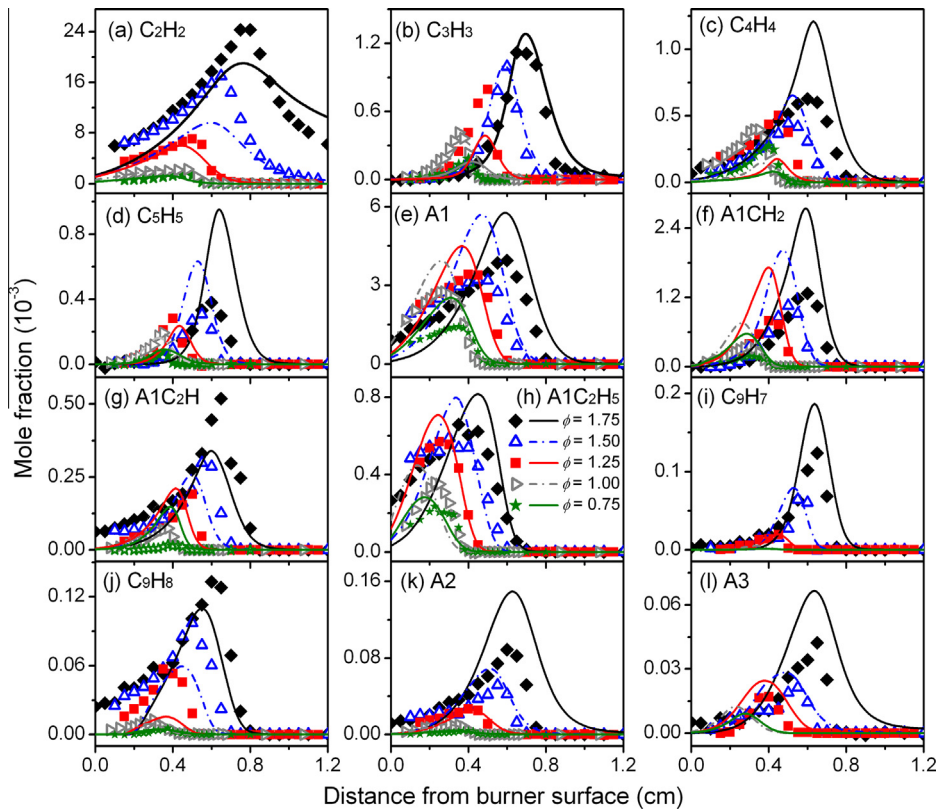


Fig. 19. Experimental (symbols) [27] and simulated (lines) mole fraction profiles of acetylene (C_2H_2), propargyl (C_3H_3), vinylacetylene (C_4H_4), cyclopentadienyl (C_5H_5), benzene ($A1$), benzyl ($A1CH_2$), phenylacetylene ($A1C_2H$), ethylbenzene ($A1C_2H_5$), indenyl (C_9H_7), indene (C_9H_8), naphthalene ($A2$) and phenanthrene ($A3$) in the premixed flames of toluene at five equivalence ratios from 0.75 to 1.75.

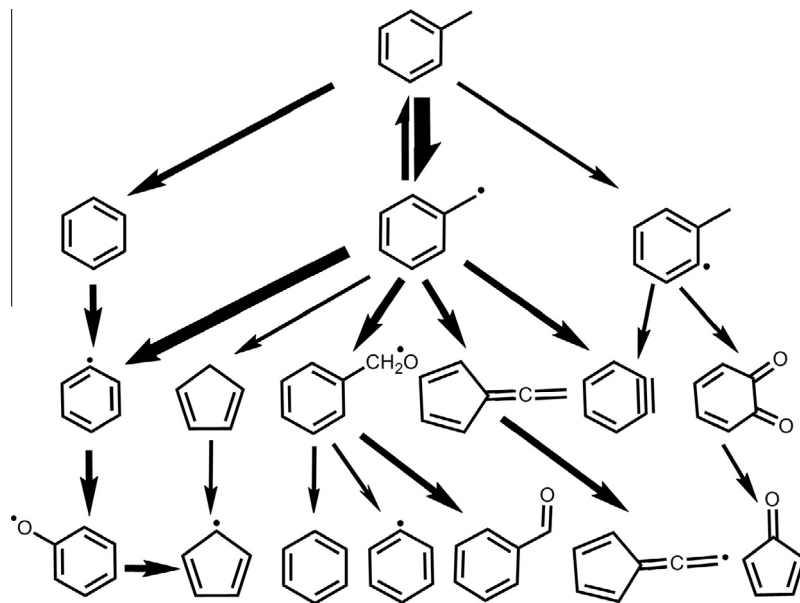


Fig. 20. The reaction network of toluene oxidation in the premixed flame of toluene at $\phi = 1.90$.

$A1\cdot$, $A1CH_2O$, C_7H_6 and $o-C_6H_4$. Due to the abundant production of H atom in the $\phi = 1.90$ flame, the reaction between $A1CH_2$ and H (R37) becomes the dominant consumption pathway of $A1CH_2$. The subsequent oxidation of $A1\cdot$ and decomposition of $A1CH_2O$ are similar to those in the JSR oxidation. Moreover due to the very rich reaction circumstance, the consumption of $A1CH_2$ in the ϕ

$= 1.90$ flame has similarity to that in the flow reactor pyrolysis at similar pressures. The ROP analysis shows that 32% of $A1CH_2$ is consumed by unimolecular decomposition reactions to form $C_7H_6 + H$, $o-C_6H_4 + CH_3$ and $C_5H_5 + C_2H_2$. The major decomposition pathways of C_7H_6 and $o-C_6H_4$ are very close to those in the flow reactor pyrolysis in Part I [1].

Figure 17(e–p) shows the experimental and simulated mole fraction profiles of some C₁–C₅ hydrocarbon species. The model can capture the formation of most species, except for CH₃ and C₅H₆. The ROP analysis shows that at the rich condition, about 30% of CH₃ comes from the reaction of A1CH₂ and H (R40), 20% from the decomposition of ketene (CH₂CO, R41) and 20% from the reaction of singlet methylene radical (CH₂). The major formation source of C₅H₆ is the combination of C₅H₅ and H, and the rest of C₅H₆ comes from the decomposition reactions of A1OH (R42) and A1O (R43).



Figure 18 presents the experimental and simulated mole fraction profiles of some representative large aromatic species in the $\phi = 1.90$ flame. The formation pathways of most large MAHs and PAHs are similar to those in the flow reactor pyrolysis at similar pressures, except the main formation pathway of A2. The ROP analysis shows that about 43% of A2 in the $\phi = 1.90$ flame is produced from the reaction sequence A1 $-$ + C₄H₂ \rightarrow A2 -1 /A2 -2 \rightarrow A2, rather than the reaction sequence C₉H₇ + CH₃ \rightarrow 1-methylindane (C₉H₇CH₃) \rightarrow A2 that dominates the formation of A2 in the flow reactor pyrolysis in Part I [1]. The most possible reason for this difference is that in the flames, C₉H₇ is not very easy to be produced and can be quickly consumed by the oxidation reactions by OH and O, instead of producing C₉H₇CH₃.

In the $\phi = 0.75$ flame, A1CH₃ is mainly consumed via the H-atom abstraction reactions by OH, O and H to produce A1CH₂ and C₆H₄CH₃. Among the H-atom abstraction reactions, those by OH and O are more favored. The reactions between A1CH₃ and O to produce OC₆H₄CH₃, HOOC₆H₄CH₃ and C₅H₅CH₃ also become significant, and contribute 8% together to the consumption of

A1CH₃. About half of A1CH₂ is consumed by the reaction with O to form A1CH₂O (R31), and the rest mainly produces A1 $-$ and A1CH₃ via (R40) and the reverse reaction of (R22), respectively. The consumption pathways of A1CH₂O are similar to those in the JSR oxidation. The consumption of C₆H₄CH₃ in the $\phi = 0.75$ flame is also very similar to that in the JSR oxidation, which mainly proceeds via oxidation reaction sequences to produce o-C₆H₄O₂, OC₆H₄CH₃ and C₅H₄O.

3.6. Ignition delay times in shock tube and rapid compression machine

There are a great deal of studies on the measurement of ignition delay times at different temperatures, pressures and equivalence ratios, either in shock tube or in rapid compression machine (RCM). For the shock tube simulation, the simulated ignition delay time is defined as the point of maximum temperature rising, when the OH concentration reaches half of its maximum. The RCM simulation was performed with the Senkin code [79] in conjunction with Chemkin II program [80]. The compression heating and post-compression heat lose were considered by using the volume-time histories which are evaluated from the pressure-time histories of nonreactive mixtures, as suggested by Mittal and Sung [81]. The simulated ignition delay time is defined as the occurrence of an inflection point in the pressure-time history during the ignition-induced pressure rising.

Figure 21 presents the experimental [29–32,34] and simulated ignition delay times of toluene in shock tube. Figure 21(a–c) shows the results at pressures from 1 to 6.81 atm. It can be observed that this model can properly reproduce the ignition delay times at these pressures. The ignition delay times of toluene at pressures higher than 10 atm have been measured by Davidson et al. [31] and Shen et al. [34]. Both the two sets of high pressure data were used to validate this model, as shown in Fig. 21(d–f). The simulated results are in reasonably good agreement with the experimental data of Shen et al. [34] at 12 and 50 atm. From Fig. 21(d), it can be seen that the measured ignition delay times at 12 atm only show little dependence on the change of equivalence ratios, which is also the case

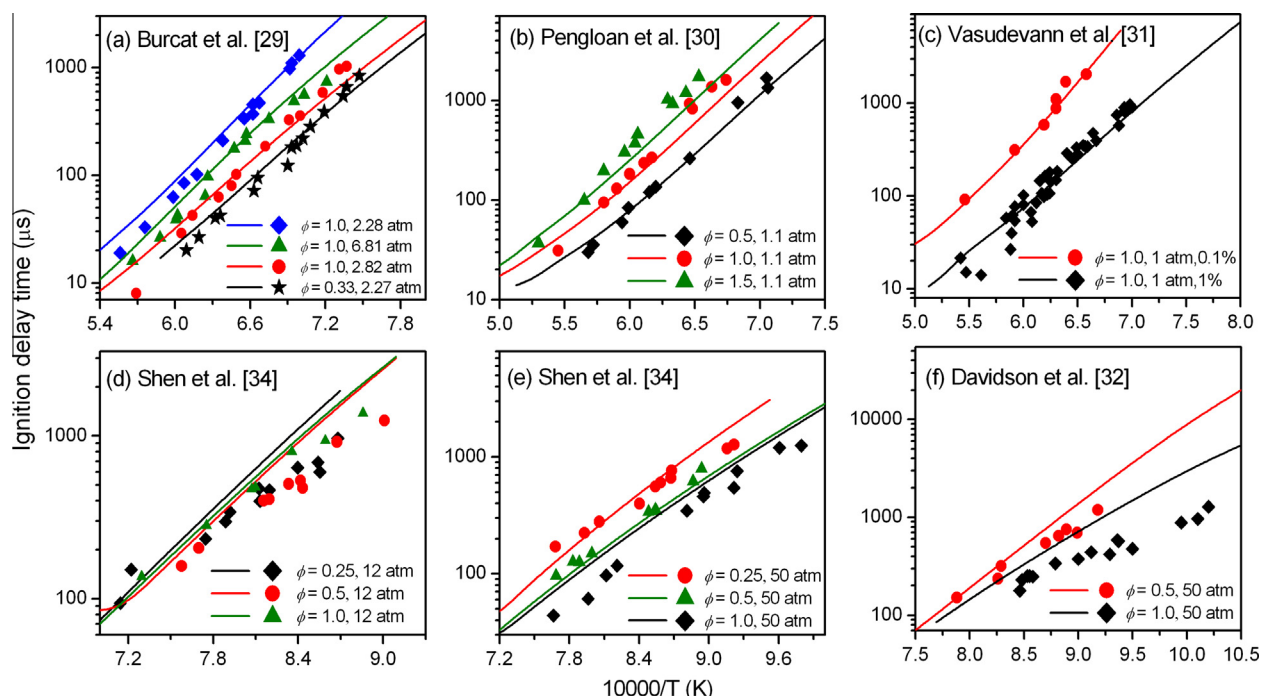


Fig. 21. Experimental (symbols) [29–32,34] and simulated (lines) ignition delay times of toluene in shock tube at different temperatures, pressures and dilutions.

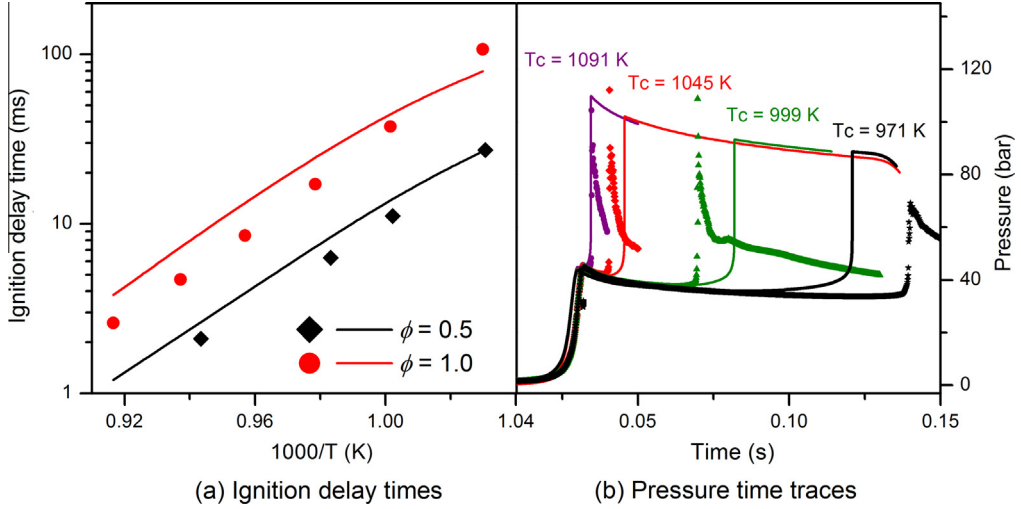


Fig. 22. Experimental (symbols) [33] and simulated (lines) (a) ignition delay times of toluene in rapid compression machine at 45 bar and $\phi = 0.5, 1.0$; (b) pressure–time traces of toluene ignition in rapid compression machine at $\phi = 1.0$ and different compression temperatures.

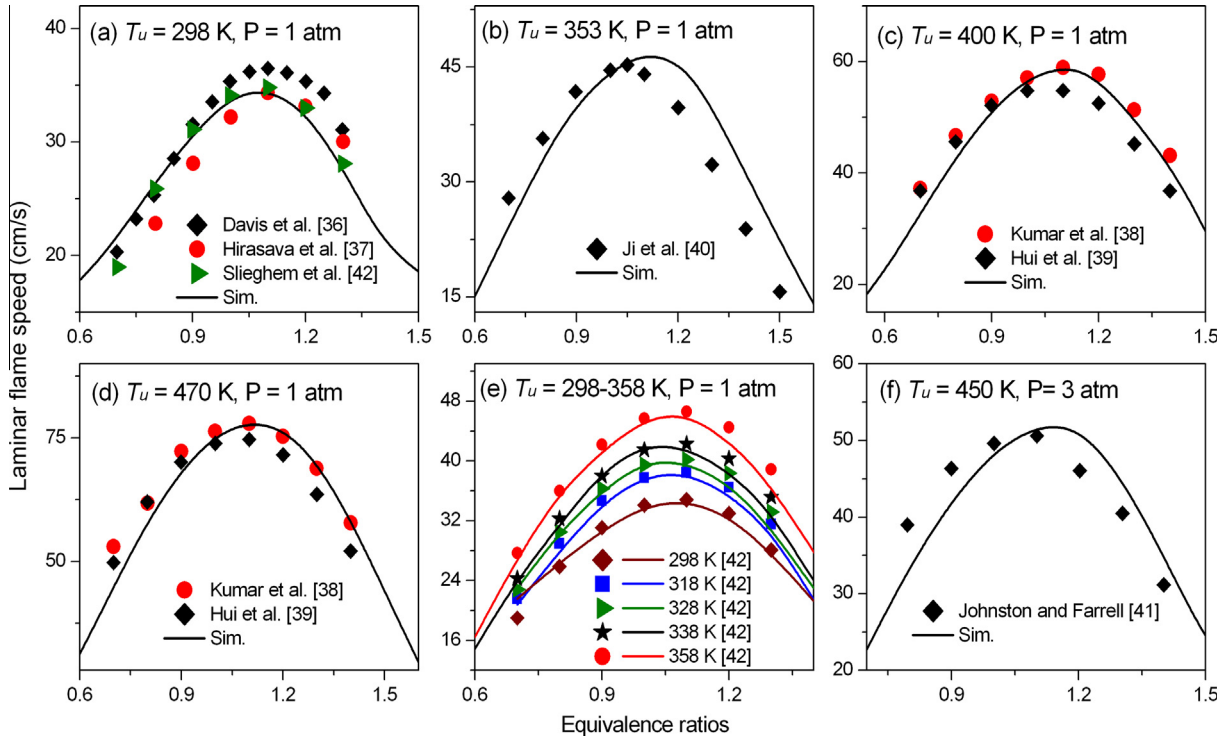


Fig. 23. Experimental (symbols) [36–42] and simulated (lines) laminar flame speeds of toluene at different pressures and initial temperatures.

for the simulated results. In Fig. 21(e and f), the 50 atm data measured by Shen et al. [34] and Davidson et al. [31] were compared to the simulation results, respectively. For the data of Shen et al. [34], this model can achieve a good simulation at lean conditions, but over-predicts the ignition delay times at $\phi = 1.0$ by less than a factor of 1.5, although it can capture the trend at different temperatures. For the data of Davidson et al. [31], the discrepancy between the experimental and simulated results becomes larger, especially at temperatures below 1050 K. Shen et al. [34] have compared their experimental results with those of Davidson et al. [31] at same conditions, and found that the overall activation energy evaluated from the data of Davidson et al. [31] is

approximately half of their result. The reason for this discrepancy was attributed by Shen et al. [34] to a pre-ignition pressure rise observed in the experiment of Davidson et al. [31], possibly caused by the contamination of the shock tube or other non-ideal effects.

Mittal and Sung [33] investigated the autoignition of toluene in a RCM at conditions relevant to HCCI combustion. The experiments were performed at pressures from 25 to 45 bar and temperatures from 920 to 1100 K. In this work, the experimental results at 45 bar and two equivalence ratios were simulated. As shown in Fig. 22(a), it can be seen that the agreement between experimental and simulated results is good with consideration of the experimental uncertainties. The simulated pressure traces at $\phi = 1.0$ were also

compared to the experimental results, as shown in Fig. 22(b). Generally, this model can reasonably predict the pressure rises as well as the inflection points.

3.7. Laminar flame speeds

There are a great deal of studies on the measurement of laminar flame speeds of toluene [36–42]. Most of the studies were performed at 1 atm with the initial temperatures ranging from 298 to 470 K, while only Johnston and Farrell [41] measured the laminar flame speeds of toluene at 3 atm with the initial temperature of 450 K. In this work, the model was also validated against these data. The simulation was performed with the Premixed Laminar Flame-Speed Calculation module in the Chemkin-Pro software [43], over a computational domain of 15 cm. The Soret effect was considered, and the mixture-averaged transport properties were used. The maximum computational grids were set as large as possible to ensure an enough refinement. Figure 23(a-d) presents the experimental and simulated laminar flame speeds of toluene at 1 atm and the initial gas temperatures of 298, 353, 400 and 470 K. Figure 23(e) presents the experimental and simulated laminar flame speeds of toluene at 1 atm with the initial temperature from 298 to 358 K. Figure 23(f) presents the experimental and simulated laminar flame speeds of toluene at 3 atm with the initial temperature of 450 K. Generally this model can reproduce the flame speed data within the experimental uncertainties, except the slight under-predictions of the rich sides for the data of Davis and Law [36] and Ji et al. [40].

4. Conclusions

The kinetic model developed in Part I in this serial work was validated using a vast amount of experimental data of toluene pyrolysis and oxidation reported in recent years, including species profiles in shock tube pyrolysis and oxidation, JSR oxidation at low temperature, atmospheric pressure flow reactor oxidation and low pressure premixed flames, and global combustion parameters such as ignition delay times and laminar flame speeds. The validated experimental data cover a wide range of conditions from low to high temperatures, subatmospheric to high pressures, very lean to pyrolysis conditions.

The dominant consumption pathways of A1CH₃ and A1CH₂ in the shock tube pyrolysis are quite similar to those in the flow reactor pyrolysis discussed in Part I. The slight differences mainly result from the different experimental conditions. Under shock tube pyrolysis conditions, C₂H₂ and C₄H₂ are two abundant products and are mainly produced from the stepwise decomposition of A1CH₂. Moreover, the main formation pathways of representative PAHs are also similar between the shock tube pyrolysis and the flow reactor pyrolysis. The dominant consumption pathways of A1CH₃ in the low temperature JSR oxidation have some major differences from those at intermediate and high temperatures. In the premixed flames, the consumption of A1CH₃ and A1CH₂ shows significant dependence on equivalence ratios. In the rich flames, the chemistry of A1CH₃ has some similarities to that in the pyrolysis. As the equivalence ratio decreases, oxidation reactions become dominant, and the chemistry of A1CH₃ is similar to that in the oxidation in homogeneous reactors such as JSR and shock tube. In the very rich flames, PAHs can be abundantly formed and their oxidation rate is slow. In the stoichiometric and lean flames, the formation of PAHs is not that easy, and their consumption rates are much quicker than those in rich flames.

The work also highlighted the importance of A1CH₂ chemistry and A1 and C₅H₆ sub-mechanisms in the pyrolysis and oxidation of toluene. To get a more reliable A1CH₂ chemistry and A1 and

C₅H₆ sub-mechanisms, the present model was also validated against the experimental data on the decomposition of A1CH₂ and the pyrolysis and oxidation of A1, A1OH and C₅H₆. The good agreement between the experimental and simulated results in this work indicates that the present model can be used to simulate a wide range of combustion conditions and also as a start point for developing the kinetic models of larger aromatic fuels.

Acknowledgments

The research at USTC leading to these results has received funding from National Natural Science Foundation of China (51106146), National Basic Research Program of China (973 Program) (2013CB834602), Anhui Provincial Natural Science Foundation (1408085J09), Fundamental Research Funds for the Central Universities (WK2320000020, WK2320000028) and Chinese Academy of Sciences. The research at CNRS leading to these results has received funding from the European Research Council under the European Community's Seventh Framework Programme (FP7/2007–2013)/ERC grant agreement n° 291049 – 2G-CSafe. We are also grateful to Mr. Zhandong Wang, Yizun Wang and Alexandre Marchal for technical assistance.

Appendix A. Supplementary material

Supplementary data associated with this article can be found, in the online version, at <http://dx.doi.org/10.1016/j.combustflame.2014.07.011>.

References

- [1] W.H. Yuan, Y.Y. Li, P. Dagaut, J.Z. Yang, F. Qi, Combust. Flame 162 (1) (2014) 3–21, <http://dx.doi.org/10.1016/j.combustflame.2014.07.009>.
- [2] R.D. Smith, J. Phys. Chem. 83 (1979) 1553–1563.
- [3] K.M. Pamidimukkala, R.D. Kern, M.R. Patel, H.C. Wei, J.H. Kiefer, J. Phys. Chem. 91 (1987) 2148–2154.
- [4] M.B. Colket, D.J. Seery, Proc. Combust. Inst. 25 (1994) 883–891.
- [5] R.A. Eng, A. Gebert, E. Goos, H. Hippler, C. Kachiani, Phys. Chem. Chem. Phys. 4 (2002) 3989–3996.
- [6] R. Sivaramakrishnan, R.S. Tranter, K. Brezinsky, J. Phys. Chem. A 110 (2006) 9388–9399.
- [7] R. Sivaramakrishnan, R.S. Tranter, K. Brezinsky, J. Phys. Chem. A 110 (2006) 9400–9404.
- [8] M.A. Oehlschlaeger, D.F. Davidson, R.K. Hanson, Proc. Combust. Inst. 31 (2007) 211–219.
- [9] T.C. Zhang, L.D. Zhang, X. Hong, K.W. Zhang, F. Qi, C.K. Law, T.H. Ye, P.H. Zhao, Y.L. Chen, Combust. Flame 156 (2009) 2071–2083.
- [10] F. Lannuzel, R. Bounaceur, R. Michels, G. Scacchi, P.-M. Marquaire, J. Anal. Appl. Pyrol. 87 (2010) 236–247.
- [11] L.D. Zhang, J.H. Cai, T.C. Zhang, F. Qi, Combust. Flame 157 (2010) 1686–1697.
- [12] B. Shukla, A. Susa, A. Miyoshi, M. Koshi, J. Phys. Chem. A 111 (2007) 8308–8324.
- [13] A. Matsugi, A. Miyoshi, Proc. Combust. Inst. 34 (2013) 269–277.
- [14] K. Brezinsky, T.A. Litzinger, I. Glassman, Int. J. Chem. Kinet. 16 (1984) 1053–1074.
- [15] K. Brezinsky, A.B. Lovell, I. Glassman, Combust. Sci. Technol. 70 (1990) 33–46.
- [16] J.L. Emdee, K. Brezinsky, I. Glassman, J. Phys. Chem. 96 (1992) 2151–2161.
- [17] S.D. Klotz, K. Brezinsky, I. Glassman, Proc. Combust. Inst. 27 (1998) 337–344.
- [18] P. Dagaut, G. Pengloan, A. Ristori, Phys. Chem. Chem. Phys. 4 (2002) 1846–1854.
- [19] I.D. Costa, R. Fournet, F. Billaud, F. Battin-Leclerc, Int. J. Chem. Kinet. 35 (2003) 503–524.
- [20] R. Sivaramakrishnan, R.S. Tranter, K. Brezinsky, Combust. Flame 139 (2004) 340–350.
- [21] R. Bounaceur, I. Da Costa, R. Fournet, F. Billaud, F. Battin-Leclerc, Int. J. Chem. Kinet. 37 (2005) 25–49.
- [22] R. Sivaramakrishnan, R.S. Tranter, K. Brezinsky, Proc. Combust. Inst. 30 (2005) 1165–1173.
- [23] W.K. Metcalfe, S. Dooley, F.L. Dryer, Energy Fuels 25 (2011) 4915–4936.
- [24] A. Hamins, K. Seshadri, Combust. Flame 68 (1987) 295–307.
- [25] V. Detilleux, J. Vandooren, J. Phys. Chem. A 113 (2009) 10913–10922.
- [26] Y.Y. Li, L.D. Zhang, Z.Y. Tian, T. Yuan, J. Wang, B. Yang, F. Qi, Energy Fuels 23 (2009) 1473–1485.
- [27] Y.Y. Li, J.H. Cai, L.D. Zhang, T. Yuan, K.W. Zhang, F. Qi, Proc. Combust. Inst. 33 (2011) 593–600.
- [28] V. Detilleux, J. Vandooren, Proc. Combust. Inst. 33 (2011) 217–224.

- [29] A. Burcat, C. Snyder, T. Brabbs, Ignition Delay Times of Benzene and Toluene with Oxygen in Argon Mixtures, NASA Technical Memorandum 87312, Washington, D.C., May 1986.
- [30] G. Pengloan, P. Dagaout, N. Djebaili-Chaumeix, C.E. Paillard, M. Cathonnet, Proceedings of the Colloque Combustion Propre, Orleans, France, June 6–8 2001, pp. 9.
- [31] D.F. Davidson, B.M. Gauthier, R.K. Hanson, *Proc. Combust. Inst.* 30 (2005) 1175–1182.
- [32] V. Vasudevan, D.F. Davidson, R.K. Hanson, *Proc. Combust. Inst.* 30 (2005) 1155–1163.
- [33] G. Mittal, C.-J. Sung, *Combust. Flame* 150 (2007) 355–368.
- [34] H.-P.S. Shen, J. Vanderover, M.A. Oehlschlaeger, *Proc. Combust. Inst.* 32 (2009) 165–172.
- [35] S.S. Vasu, D.F. Davidson, R.K. Hanson, *J. Propul. Power* 26 (2010) 776–783.
- [36] S.G. Davis, C.K. Law, *Combust. Sci. Technol.* 140 (1998) 427–449.
- [37] T. Hirasawa, C.-J. Sung, A. Joshi, Z. Yang, H. Wang, C.K. Law, *Proc. Combust. Inst.* 29 (2002) 1427–1434.
- [38] K. Kumar, J.E. Freeh, C.J. Sung, Y. Huang, *J. Propul. Power* 23 (2007) 428–436.
- [39] X. Hui, A.K. Das, K. Kumar, C.-J. Sung, S. Dooley, F.L. Dryer, *Fuel* 97 (2012) 695–702.
- [40] C.S. Ji, E. Dames, H. Wang, F.N. Egolfopoulos, *Combust. Flame* 159 (2012) 1070–1081.
- [41] R.J. Johnston, J.T. Farrell, *Proc. Combust. Inst.* 30 (2005) 217–224.
- [42] L. Sileghem, V.A. Alekseev, J. Vancoillie, K.M. Van Geem, E.J.K. Nilsson, S. Verhelst, A.A. Konnov, *Fuel* 112 (2013) 355–365.
- [43] CHEMKIN-PRO 15092, Reaction Design: San Diego, 2009.
- [44] H. Wang, M. Frenklach, *Combust. Flame* 110 (1997) 173–221.
- [45] I.V. Tokmakov, J. Park, S. Gheysa, M.C. Lin, *J. Phys. Chem. A* 103 (1999) 3636–3645.
- [46] L.V. Moskaleva, L.K. Madden, M.C. Lin, *Phys. Chem. Chem. Phys.* 1 (1999) 3967–3972.
- [47] T. Seta, M. Nakajima, A. Miyoshi, *J. Phys. Chem. A* 110 (2006) 5081–5090.
- [48] Y. Sakai, A. Miyoshi, M. Koshi, W.J. Pitz, *Proc. Combust. Inst.* 32 (2009) 411–418.
- [49] M.U. Alzueta, P. Glarborg, K. Dam-Johansen, *Int. J. Chem. Kinet.* 32 (2000) 498–522.
- [50] C.A. Taatjes, D.L. Osborn, T.M. Selby, G. Meloni, A.J. Trevitt, E. Epifanovsky, A.I. Krylov, B. Sirjean, E. Dames, H. Wang, *J. Phys. Chem. A* 114 (2010) 3355–3370.
- [51] P. Frank, J. Herzler, T. Just, C. Wahl, *Proc. Combust. Inst.* 25 (1994) 833–840.
- [52] X.Q. You, D.Y. Zubarev, W.A. Lester, M. Frenklach, *J. Phys. Chem. A* 115 (2011) 14184–14190.
- [53] L.V. Moskaleva, M.C. Lin, *J. Comput. Chem.* 21 (2000) 415–425.
- [54] S. Sharma, W.H. Green, *J. Phys. Chem. A* 113 (2009) 8871–8882.
- [55] X. Zhong, J.W. Bozzelli, *J. Phys. Chem. A* 102 (1998) 3537–3555.
- [56] R.K. Robinson, R.P. Lindstedt, *Combust. Flame* 158 (2011) 666–686.
- [57] J.H. Cai, L.D. Zhang, F. Zhang, Z.D. Wang, Z.J. Cheng, W.H. Yuan, F. Qi, *Energy Fuels* 26 (2012) 5550–5568.
- [58] J.H. Cai, W.H. Yuan, L.L. Ye, Z.J. Cheng, Y.Z. Wang, L.D. Zhang, F. Zhang, Y.Y. Li, F. Qi, *Combust. Flame* 160 (2013) 1939–1957.
- [59] M.A. Oehlschlaeger, D.F. Davidson, R.K. Hanson, *J. Phys. Chem. A* 110 (2006) 6649–6653.
- [60] R. Sivaramakrishnan, M.C. Su, J.V. Michael, *Proc. Combust. Inst.* 33 (2011) 243–250.
- [61] A. Laskin, A. Lifshit, *Proc. Combust. Inst.* 26 (1996) 669–675.
- [62] A. Ristori, P. Dagaout, A.E. Bakali, G. Pengloan, M. Cathonnet, *Combust. Sci. Technol.* 167 (2001) 223–256.
- [63] A. Marchal, M. Cathonnet, P. Dagaout, M. Reuillon, M. Audinet, G. Belot, J.-F. Béziau, Proceedings of the Joint Meeting of the French and German Sections of the Combustion Institute, Mulhouse, October 1995; pp. 11–13.
- [64] A.B. Lovell, K. Brezinsky, I. Glassman, *Int. J. Chem. Kinet.* 21 (1989) 547–560.
- [65] K. Brezinsky, M. Peculian, I. Glassman, *J. Phys. Chem. A* 102 (1998) 8614–8619.
- [66] D.H. Kim, J.A. Mulholland, D. Wang, A. Violi, *J. Phys. Chem. A* 114 (2010) 12411–12416.
- [67] R.G. Butler, I. Glassman, *Proc. Combust. Inst.* 32 (2009) 395–402.
- [68] M.R. Djokic, K.M. Van Geem, C. Cavallotti, A. Frassoldati, E. Ranzi, G.B. Marin, *Combust. Flame* 161 (11) (2014) 2739–2751, <http://dx.doi.org/10.1016/j.combustflame.2014.04.013>.
- [69] J.P. Orme, H.J. Curran, J.M. Simmie, Shock tube study of 5 membered cyclic hydrocarbon oxidation, in: Proceedings of the European Combustion Meeting, Louvain-la-Neuve, Belgium, April 3–6 2005.
- [70] C. Ji, R. Zhao, B. Li, F.N. Egolfopoulos, *Proc. Combust. Inst.* 34 (2013) 787–794.
- [71] A. Comandini, K. Brezinsky, *J. Phys. Chem. A* 115 (2011) 5547–5559.
- [72] A. Comandini, T. Malewicki, K. Brezinsky, *J. Phys. Chem. A* 116 (2012) 2409–2434.
- [73] K. Narayanaswamy, G. Blanquart, H. Pitsch, *Combust. Flame* 157 (2010) 1879–1898.
- [74] M. Braun-Unkhoff, P. Frank, T. Just, *Proc. Combust. Inst.* 22 (1988) 1053–1061.
- [75] M.A. Oehlschlaeger, D.F. Davidson, R.K. Hanson, *Combust. Flame* 147 (2006) 195–208.
- [76] J.C.G. Andrae, T. Brinck, G.T. Kalghatgi, *Combust. Flame* 155 (2008) 696–712.
- [77] J.C.G. Andrae, *Fuel* 107 (2013) 740–748.
- [78] Y.R. Luo, *Comprehensive Handbook of Chemical Bond Energies*, CRC Press, Boca Raton, FL, 2007.
- [79] A.E. Lutz, R.J. Kee, J.A. Miller, Senkin: a Fortran program for predicting homogeneous gas phase chemical kinetics with sensitivity analysis, SANDIA National Laboratories Report, SAND87-8248, Livermore, CA, 1990.
- [80] R.J. Kee, F.M. Rupley, J.A. Miller, Chemkin-II: A fortran chemical kinetics package for the analysis of gas phase chemical kinetics, Sandia National Laboratories, Report No. SAND89-8009B, Livermore, CA, 1989.
- [81] G. Mittal, C.-J. Sung, *Combust. Sci. Technol.* 179 (2007) 487–530.